

OTTO VON GUERICKE UNIVERSITÄT MAGDEBURG

MASTER'S THESIS

Simulation of Brain Functional and Structural Connectivity on Empirical and Randomized Complex Networks

Supervisor:

Author:

Seyma BAYRAK

Prof. Jochen BRAUN

Dr. Philipp HÖVEL

Dr. Vesna VUKSANOVIC

*A thesis submitted in fulfilment of the requirements
for the degree of Master of Science*

in the

Bernstein Center for Computational Neuroscience Nachwuchsgruppe: Nonlinear
Dynamics and Control in Neuroscience
Integrative Neuroscience

November 2014

Declaration of Authorship

I, Seyma BAYRAK, declare that this thesis titled, 'Simulation of Brain Functional and Structural Connectivity on Empirical and Randomized Complex Networks' and the work presented in it are my own. I confirm that:

- This work was done wholly or mainly while in candidature for a research degree at this University.
- Where any part of this thesis has previously been submitted for a degree or any other qualification at this University or any other institution, this has been clearly stated.
- Where I have consulted the published work of others, this is always clearly attributed.
- Where I have quoted from the work of others, the source is always given. With the exception of such quotations, this thesis is entirely my own work.
- I have acknowledged all main sources of help.
- Where the thesis is based on work done by myself jointly with others, I have made clear exactly what was done by others and what I have contributed myself.

Signed:

Date:

“Thanks to my solid academic training, today I can write hundreds of words on virtually any topic without possessing a shred of information, which is how I got a good job in journalism.”

Dave Barry

UNIVERSITY NAME (IN BLOCK CAPITALS)

Abstract

Faculty Name
Integrative Neuroscience

Master of Science

**Simulation of Brain Functional and Structural Connectivity on Empirical
and Randomized Complex Networks**

by Şeyma BAYRAK

The Thesis Abstract is written here (and usually kept to just this page). The page is kept centered vertically so can expand into the blank space above the title too...

Acknowledgements

The acknowledgements and the people to thank go here, don't forget to include your project advisor...

Contents

Declaration of Authorship	i
Abstract	iii
Acknowledgements	iv
Contents	v
List of Figures	vii
List of Tables	viii
Abbreviations	ix
Physical Constants	x
Symbols	xi
1 Introduction	1
2 Methods and Models	4
2.1 Empirical functional and anatomical connectivity matrices	5
2.2 The Brain Graph	7
2.3 Randomization Methods	9
2.3.1 Erdős-Rényi Type Randomization	9
2.3.2 Double-Edge-Swap Type Randomization	9
2.3.3 Preserved-Degree-Distribution Type Randomization	10
2.3.4 Configuration Model Randomization	12
2.3.5 Partial Randomization	12
2.4 Network Characterizations	14
2.4.1 Network Density	14
2.4.2 Average Clustering Coefficient	15
2.4.3 Transitivity	16
2.5 FitzHugh-Nagumo Model for Neuronal Activity Simulation	17
2.5.1 FHN Model Local Dynamics	18

2.5.2	Noise Effect	20
2.5.3	Global Dynamics	21
2.5.4	FHN Time Series	22
2.6	Balloon-Windkessel Model for BOLD Activity Simulation	24
2.6.1	Hemodynamic Model	26
3	Results	29
3.1	FHN	29
4	Conclusion	37
4.0.1	Common L ^A T _E X Math Symbols	37
4.1	Getting Started with this Template	37
4.1.1	About this Template	38
4.2	What this Template Includes	38
4.2.1	Folders	38
4.2.2	Files	39
4.3	Filling in the ‘Thesis.cls’ File	41
4.4	The ‘Thesis.tex’ File Explained	41
4.5	Thesis Features and Conventions	42
4.5.1	Printing Format	42
4.5.2	Using US Letter Paper	43
4.5.3	References	43
4.5.4	Figures	44
4.5.5	Typesetting mathematics	45
4.6	Sectioning and Subsectioning	46
4.7	In Closing	46
A	Appendix Title Here	48
Bibliography		49

List of Figures

2.1	Empirical FCM and ACM	6
2.2	Empirical FCM and ACM in cortex	6
2.3	Binarizing via thresholding	8
2.4	Erdos-Renyi Example	9
2.5	Double-Edge-Swap Example	10
2.6	Degree Distribution 2D Example	11
2.7	Degree Distribution 3D Example	11
2.8	Degree Sequence Definition	12
2.9	Partial Randomization Example	13
2.10	Network Density	14
2.11	Clustering Coefficient	15
2.12	Transitivity	16
2.13	FHN Local	20
2.14	FHN Noise	21
2.15	FHN Global	22
2.16	FHN Graph	23
2.17	FHN Time Series	24
2.18	Hemodynamic Model	26
3.1	Parameter Analysis, FCM	29
3.2	Best correlated FHN simulation, FCM	30
3.3	Neural Activity Node Dynamics, FCM	30
3.4	3D Fourier Transform, FHN, FCM	31
3.5	Parameter Analysis, ACM	31
3.6	Best correlated FHN simulation, ACM	32
3.7	Neural Activity Node Dynamics, ACM	32
3.8	3D Fourier Transform, FHN, ACM	33
3.9	Parameter Analysis, BOLD	33
3.10	Best correlated BOLD simulation, FCM	34
3.11	BOLD Activity Node Dynamics, FCM	34
3.12	3D Fourier Transform, BOLD, FCM	35
3.13	Best correlated BOLD simulation, ACM	35
3.14	BOLD Activity Node Dynamics, ACM	36
4.1	An Electron	45

List of Tables

2.1 Abbreviations	13
2.2 BOLD Abbreviations	26

Abbreviations

LAH List Abbreviations Here

Physical Constants

Speed of Light c = $2.997\ 924\ 58 \times 10^8$ ms⁻¹ (exact)

Symbols

a	distance	m
P	power	W (Js ⁻¹)
ω	angular frequency	rads ⁻¹

For/Dedicated to/To my...

Chapter 1

Introduction

The purpose of this master's project is to quantify large-scale functional and structural brain networks and the comparison to resting-state functional Magnetic Resonance Imaging (fMRI). The functional brain networks are derived from simulated Blood-Oxygen-Level-Dependent (BOLD) signals, whereas the structural brain networks are obtained from Diffusion-Weighted Magnetic Resonance Imaging (DW-MRI). The project uses experimental results combined with modelling approaches and implements methods drawn from nonlinear and network science.

The functional connectivities in a typical fMRI experiment are obtained from pre-defined brain regions, whose corresponding time-series of BOLD activity display significant correlations at low-frequencies (< 0.1 Hz). The measured activity patterns are correlated and complex, but highly structured and robust. They have been observed also for brains in resting state, i.e. under no stimulations and in the absence of any stimulus-driven task. The fMRI-BOLD empirical data used in this project is obtained from the *1000 Functional Connectome Project* website <http://www.nitric.org/>). This data set is also referred as functional connectivity matrix (FCM) revealing the correlated activities among the 90 cortical and sub-cortical regions with the automated anatomical labelling (AAL) template as given in Table 1 in Appendix.

The DW-MRI technique estimates the anatomical connection probabilities among brain regions indirectly by investigating the diffusion direction of water molecules. The direction of the fiber tracks in white matter depends indirectly on the diffusion of water molecules. A DW-MRI experiment approximates the existence of a fiber track between regions of interest. The anatomical connection probability (ACP) matrix for the 90 anatomically labelled brain regions considered in this project is obtained from the study of Iturria-Medina et. al. (2008) [1]. Both anatomical and functional connectivities are considered for the same cortical and sub-cortical regions.

[1] Iturria-Medina et. al. (2008)

Statistical characterization of the functional brain networks, using methods from graph theory, has revealed some of their key topological properties such as small worldness, modularity or resilience to the attacks [BUL09]. This project studies these properties both for functional and structural brain networks arising from modelled intrinsic brain dynamics. In particular, such conditions that distinguish obtained network topologies from that of random networks will be explored. Several randomization procedures will be considered. They include, but are not limited to random networks of Erdos-Renyi-type with the same number of nodes and links as in the empirically derived case. This approach will provide a deeper insight into the underlying processes involved in the observed functional connectivity and their relations to the coupling topology, i.e., brain structural connectivity.

Despite important progress over the past few years, the way how functional connectivity arises from the complex anatomical connectivity still remains poorly understood [VUK14]. Existing models of resting-brain dynamics hypothesize that functional interactions result from a complex interplay between intrinsic brain dynamics and underlying structural connections [RUB09]. In particular, these models explore the range of conditions at which functional networks emerge from anatomical connections, the role of multiple time-scales in the formation of functional-connectivity networks [HON07], time delays in the signal propagation between the network nodes as well as the system noise [GHO08, GHO08a], local network oscillations [DEC09, CAB11] and structural disconnection [CAB12].

In this project, the model of resting-state brain activity will be based on the models previously proposed in [VUK13, VUK14]. The key ingredients are coupling topologies of the time-delayed functional interactions which are scaled by the global coupling strength c and are subject to the Gaussian white noise. The time-delay in the model arises as the natural consequence of a finite speed of signal propagation along axons. Therefore, velocity v , representing biophysically realistic axonal signal propagation [GH008, GHO08a, DEC09] is another important ingredient of the model.

The rest of the master's thesis is organized in the following order : Section 2 will introduce the empirical data sets of FCM and ACM used in this project. This section will further explain the randomization methods used to construct random graphs. Characterization of those brain networks by using methods of network science [RUB09, STA10, NEW10, RUB11] will be done by quantifying global and local network properties such as network density, clustering coefficient, small-worldness etc.. Section 2 will introduce the FitzHugh-Nagumo (FHN) model of neuronal interactions [14,15 VUK13ten bak!] and Balloon-Windkessel hemodynamic model [16 -VUK13ten bak]. Section 3 will illustrate

the effect of coupling strength c and signal propagation velocity v on the empirically derived brain networks and reshuffled networks. Additionally, such parameter regions will be identified at which the network properties of the empirical data differ from that of random graphs. Section 4 will conclude the master's thesis.

Chapter 2

Methods and Models

Graph theory is a mathematical field applicable to a considerable diversity of complex systems such as markets, ecosystems, computer circuits, and gene-gene interactions [1]. A graph is defined as an ensemble of vertices (nodes) that are linked with edges. If the edges connect the nodes in a specified direction, the graph is referred to as *directed*, otherwise *undirected*. Moreover, the edges can be assigned a weight yielding a *weighted* graph. A graph with edges of uniform weight is called an *unweighted* graph.

Network science incorporates graph theory applied on a distinct complex domain. Unlike classical graph theory, network science primarily deals with real life networks that are large and complex - neither uniformly random nor ordered [2]. The neuro-anatomical and neuro-physiological data sets derived from DW-MRI and fMRI-BOLD techniques can be constructed as such large-scale complex brain graphs that are undirected and unweighted. Nodes in large-scale brain networks usually represent brain regions, while edges represent anatomical, functional or effective connections [3].

A brain network can be statistically described in terms of its topology, i.e. solely in terms of its connectivity and independently of spatial positions of nodes and edges. Topological measures described in previous studies capture local and global properties of a network, e.g. local and global efficiency, clustering coefficient, transitivity and small-worldness [4–7].

Methods of graph theory applied to structural and functional systems have shown that both share typical features of many complex networks [8–11]. However, the essential features of brain's connectivity still remain ambiguous both for functional and structural maps. This project aims to investigate whether the brain does not behave as a completely random circuitry. This idea will be tested by comparing brain graphs to the randomized networks as it was previously noticed by Bullmore and Bassett [12]. The majority

of random graphs here are inspired by Erdős-Rényi type random networks and the configuration model.

In this section, the construction of brain graphs based on empirical functional connectivity matrix (FCM) and anatomical connectivity matrix (ACM) will be first introduced. Then, the topological characteristics of all graphs will be statistically measured and those topological measures will be interpreted neuro-biologically. In particular, it is aimed to explore under which conditions that brain network topologies distinguish from random networks. This approach is expected to provide a deeper insight into the underlying process involved in the observed functional and structural brain connectivity.

2.1 Empirical functional and anatomical connectivity matrices

The functional-magnetic-resonance-imaging (fMRI) is a widely used method to detect the blood-oxygen-level-dependent (BOLD) contrast in the brain. The fMRI-BOLD contrast is used to interpret the neuronal activity in the respective voxel, which can be considered as a rectangular volume in brain defined for the imaging studies. The ongoing firing activity of neurons requires energy and it is supplied by neighboring blood cells via oxygen and glucose release into the nerve cells. The deviations in deoxygenation level, cerebral flow and volume in blood vessels due to neuronal activity, known as *hemodynamic process*, cause a change in the detected fMRI-BOLD signal strength. The functional connectivity matrix (FCM) represents correlation coefficients of these fMRI-BOLD signals detected from the pre-defined brain regions with voxels.

The resting state empirical FCM used in this project is obtained from the *1000 Functional Connectome Project* website (<http://www.nitric.org/>). The human brain is segmented into $N = 90$ cortical and sub-cortical regions according to the Tzourio-Mazoyer brain atlas with the automated anatomical labeling (AAL) template [13], such that regions with index $n = \{1, 2, \dots, 45\}$ lie on the right hemisphere, whereas $n = \{46, 47, \dots, 90\}$ on the left. The fMRI-BOLD activity is measured from all voxels in an AAL region for 7.5 min of acquisition time. Once the fMRI-BOLD mean time-series are obtained for all AAL regions, then the FCM is obtained by calculating the Pearson correlation coefficients of timeseries between all pairs in 90 AAL regions. Therefore the size of FCM is $N \times N = 90 \times 90$. To be more precise, BOLD-fMRI signal is averaged for the same subject over voxels in an AAL region, and FCM is averaged over all subjects at the end.

The diffusion-weighted magnetic-resonance-imaging (DW-MRI) technique estimates the anatomical connection probabilities among brain regions by investigating the diffusion direction of water molecules within a voxel. The direction of the fiber tracks in white matter depends on the diffusion pattern of water molecules. A DW-MRI experiment approximates the existence of a fiber track between regions of interest. The anatomical connectivity matrix (ACM) used in this project is obtained from the study of Iturria-Medina et. al. [14] and it is based on the same $N = 90$ AAL regions as in the FCM described above. The size of ACM is also $N \times N = 90 \times 90$, and each value reveals the probability of 2 AAL regions being connected via axonal fibers.

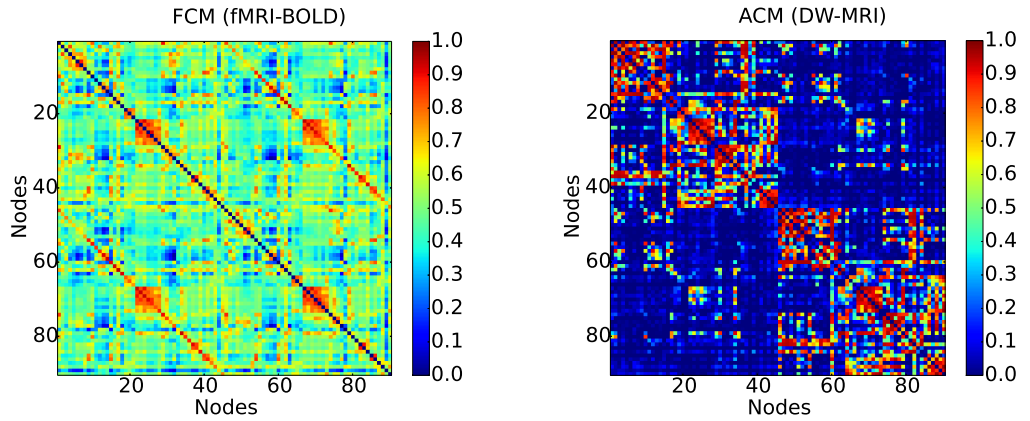


FIGURE 2.1: Empirical functional and anatomical connectivity maps of human cortex, FCM obtained from fMRI-BOLD technique (on the left) and ACM obtained from DW-MRI (on the right). The colorbars exhibit correlation coefficients and probability values in FCM and ACM, respectively.

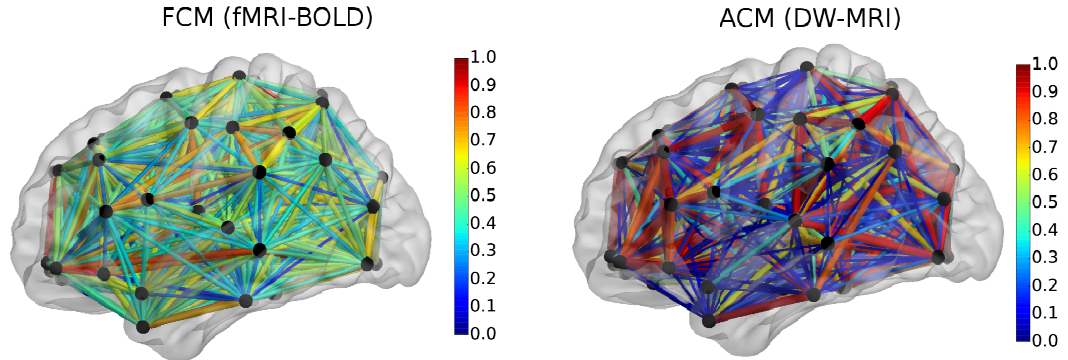


FIGURE 2.2: 3D sagittal visualization of FCM and ACM on the human cortex with the BRAINNET VIEWER [15].

Figure 2.1 represents empirically captured FCM and ACM. All correlation coefficients in FCM appear in the range $[0,1]$ as well as all probability values in ACM. Both matrices are symmetric. A correlation value close to 1 in FCM indicates that the quantified functional activities of corresponding nodes highly resemble each other. A probability value close

to 1 in ACM demonstrates that corresponding nodes are most likely connected by fiber tracks in white matter. Although some node pairs are not anatomically coupled at all in ACM (cold colors), they could be functionally coupled in FCM (hot colors).

FCM and ACM are embedded in human cortex in Figure 2.2 [15]. All nodes are presented with equal size and black color independent of their topological properties. However, edges have different thickness and color distribution according to correlation coefficients and probability values with respect to FCM and ACM.

2.2 The Brain Graph

The brain graphs considered here are derived from two sets of empirical brain connectivity maps: FCM and ACM obtained from fMRI-BOLD and DW-MRI techniques, respectively. Those data sets represent measurements from $N = 90$ cortical and subcortical regions labeled with AAL, represented by nodes in the graph. The nodes can be connected to each other by means of "edges". If the graph is constructed on the FCM, edges are interpreted as correlation strengths between the functional BOLD activity of two nodes. If the graph is built on the ACM, an existing edge is considered as the probability of two nodes to be structurally connected by fiber tracks in white matter.

The brain graphs in this project are generated through binarizing the functional connectivity matrix (FCM) and anatomical connectivity matrix (ACM). Binarization here means converting all the values in a given matrix into 1's and 0's via thresholding. Because of the nature of their definition, both empirical data sets have values between 0 and 1, reflecting a correlation strength in case of FCM or a probability value in case of ACM. We arbitrarily define a threshold value r for the strength of correlations in FCM. Then, the values greater and equal to r are assigned the value 1, while others are set to 0. This thresholding is applied by means of the strength of probability value, p , for the ACM. The binarized matrix is the basis of brain graph construction, and it is commonly known as *adjacency matrix*. The NETWORKX software package in PYTHON is used to build graphs given adjacency matrices. Neither the direction of functional or anatomical connectivity between nodes, nor any other values apart from 0 and 1 are encoded in the adjacency matrices, so that the resulting graphs are considered as "undirected" and "unweighted". In other words, all existing edges are thought to be of uniform weight and nodes interact both ways along an edge connecting them.

Figure 2.1 illustrates the exemplary construction of a brain graph from the FCM. All correlation values among the cortical and sub-cortical regions in the empirical fMRI-BOLD data lie between 0 and 1. 3D axial cortex visualization represents only the

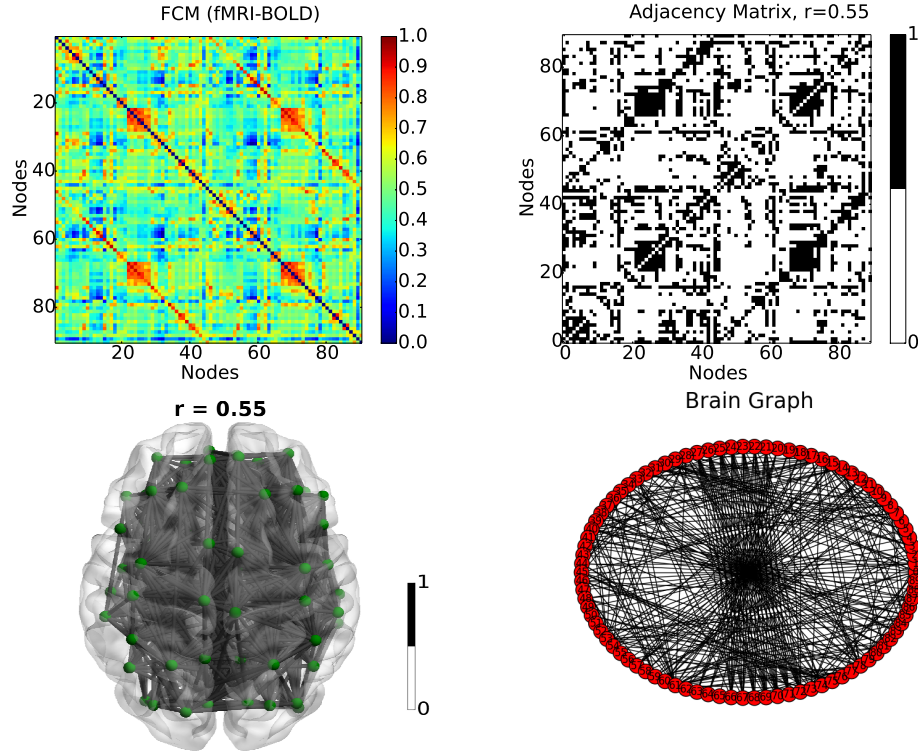


FIGURE 2.3: How to build a brain graph : The empirical data matrix derived from fMRI-BOLD technique (on the upper left) is binarized via a threshold value $r = 0.55$ and its corresponding adjacency matrix (on the upper right). The black spots represent 1's indicating edges between nodes, whereas the white squares represent 0's implying no edge at all. The adjacency matrix is embedded on human cortex axially (on the lower left) with BRAINNET VIEWER [15] and the brain graph derived from the adjacency matrix with NETWORKX (on the lower right).

existing edges with black edges among the nodes. The adjacency matrix (AM) is filled out only with 1's and 0's indicating functionally connected and unconnected nodes, whose correlated BOLD activity is equal to or greater than $r = 0.55$. The algorithm NETWORKX builds the corresponding graph of an adjacency matrix. The AM obtained from an ACM would look similar, but would represent the probability of two nodes to be anatomically connected above a predefined threshold p .

The following sections will cover randomization methods reshuffling the brain graphs and introduce some of the topological concepts characterizing brain graphs as well as random networks.

2.3 Randomization Methods

2.3.1 Erdős-Rényi Type Randomization

Given a total number of nodes N , Paul Erdős and Alfréd Rényi produced an undirected graph $G(N, P)$, in which the presence of any edge between two nodes is assigned a probability P . The average total number of edges L in an Erdős-Rényi type random graph is $\binom{N}{2}P$, with a binomial distribution for the number of edges per node.

New randomization techniques arise through modifying the Erdős-Rényi method, e.g. given N and L , a graph $G(N, L)$ can be picked uniformly random out of set of all potential graphs having N nodes and L edges. The probability for a graph to be picked among all the others is $\frac{L}{\binom{N}{2}}$. One can study the various aspects of $G(N, P)$ and $G(N, L)$ even more detailed, but for the sake of simplicity, Erdős-Rényi model will not discussed further here.

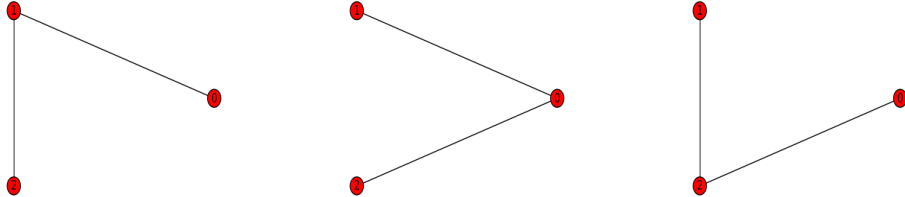


FIGURE 2.4: An illustration of the set of all $G(N, L)$ type random graphs with $N = 3$ and $L = 2$.

Figure 2.2 illustrates all possible graphs having 3 nodes and 2 edges. One of those 3 simple graph is chosen uniformly random for the $G(N, L)$ randomization type, so that each graph is chosen with probability $P = \frac{1}{3}$.

The $G(N, L)$ type randomization is the first method used to derive random graphs from the adjacency matrices of FCM and ACM in this project. Both matrices have $N = 90$ nodes, however L changes for each brain graph according to the applied threshold level and therefore is always recalculated.

2.3.2 Double-Edge-Swap Type Randomization

The *degree* k_i of a node i is defined as the number of edges connected to that node. The double-edge-swap method manipulates a given graph by swapping two existing edges among four nodes, while keeping the node degrees fixed.

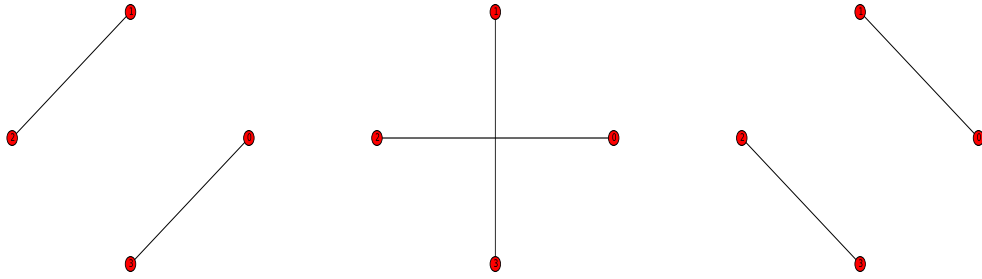


FIGURE 2.5: Swapping edges between 2 paired nodes

Figure 2.3 illustrates randomly chosen double edges in a sample graph to be swapped. After the existing edges are removed, the new pair of nodes are rewired. The degree of each node is the same before and after swapping; degrees of nodes $k_1 = 1$, $k_2 = 1$, $k_3 = 1$, $k_4 = 1$ are all fixed in each graph. Although the randomly constructed graphs with the double-edge-swap method are expected to have same degrees, the latter is not a unique property identifying a graph.

The *degree distribution* is the probability distribution of node degrees over the whole graph. Conservation of each k_i preserves the degree distribution, however, preserving degree distribution does not guarantee to fix k_i values. We will discover in the next section how to preserve degree distribution by altering node degrees.

2.3.3 Preserved-Degree-Distribution Type Randomization

The preserved-degree-distribution method randomizes a given network by adding-removing or rewiring its edges randomly while recovering its degree distribution $P(k)$. The idea is to reassign edge indices in the graph, meaning that the degree of individual nodes may change. $P(k)$ is defined with the following equation,

$$P(k) = \sum_{k' \geq k} p(k') \quad (2.1)$$

where $p(k')$ is the probability of a node to have degree number k' [16].

The algorithm is thought to add-remove new nodes to a given graph while preserving $P(k)$ as shown in Figure 2.6. However, we randomize our brain graph with a conserved

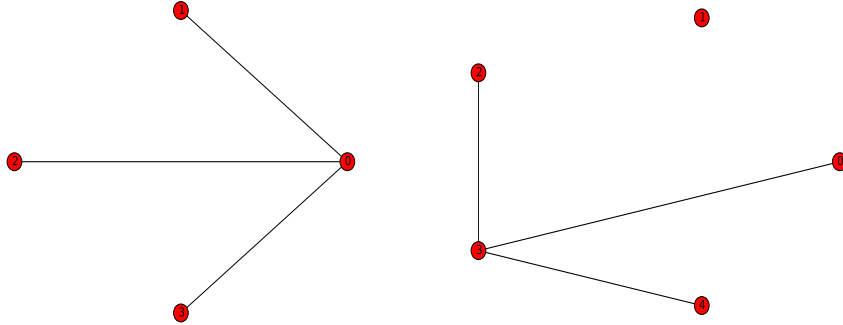


FIGURE 2.6: Reconstruction of a given graph (on the left) with degree-distribution-preservation model (on the right). $k_i = \{3, 1, 1, 1\}$ in the original graph and $k_i = \{1, 0, 1, 3, 1\}$ in the randomized graph.

total number of nodes N as well as $P(k)$. The figure is given only for a better visualization in order to distinguish preserved-degree-distribution randomization method and configuration model randomization, which will be introduced in the next section.

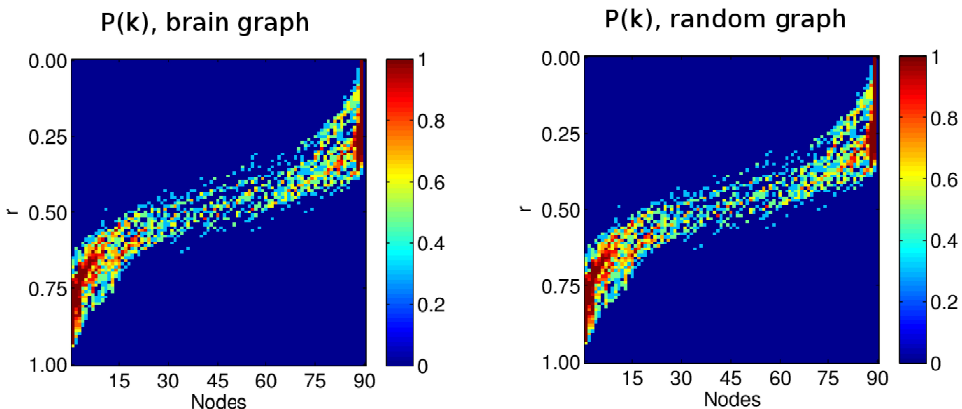


FIGURE 2.7: Heat maps for degree distributions of the brain graph obtained from FCM (on the left), and of the randomized graph with preserved-degree-distribution tool (on the right). Colorbars are in logarithmic scale with lower and upper limits : $[\log_{10} 10^0, \log_{10} 10^1]$

$P(k)$ is a global topological measure for a network, it can be illustrated over all nodes in the whole graph as in Figure 2.7. Node indexes are labeled on x axis on heat maps, threshold r values for adjacency matrices are given on y axis. The preserved-degree-distribution method generates successfully a random graph with the same $P(k)$ as in the brain graph.

2.3.4 Configuration Model Randomization

The *degree sequence* of a graph is either its ascending or descending sequence of node degrees. The configuration model generates a random graph with a given degree sequence. The direct implementation of this model is to assign edges to the nodes randomly until the desired degree sequence is matched. The resultant random graph is expected to be a node-index-shuffled version of the original graph. However, these algorithms are non-trivial due to the occurrence of self-loops (node is connected to itself) and parallel edges (multiple edges connecting two nodes), which are both undesirable graph properties in this project.

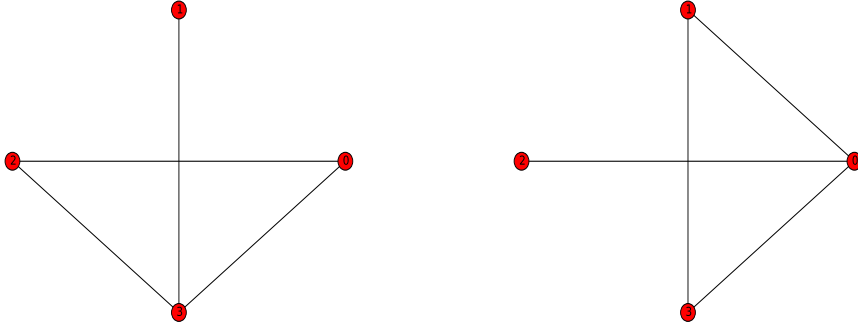


FIGURE 2.8: The degrees of the nodes in the original graph (on the left): $k_0 = 2$, $k_1 = 1$, $k_2 = 2$, $k_3 = 3$ and that of the randomized graph (on the right) : $k_0 = 3$, $k_1 = 2$, $k_2 = 1$, $k_3 = 2$. The degree sequence in non-increasing order in both graphs : $\{3, 2, 2, 1\}$

Figure 2.8 points out the relevance of the degree sequence to the node degrees. Moreover, one should not confuse degree distribution and degree sequence.

The configuration model variant used here is the expected-degree-graph method, which excludes self-loops and parallel edges. This algorithm receives the list of the expected degree sequence as an input $(k_u, k_v, k_m, k_l, \dots)$, and assigns edges between nodes with a predefined probability $P_{uv} = \frac{k_u k_w}{\sum_i k_i}$. This method does not guarantee to construct graphs with exactly the same given degree sequence but with the closest possible sequence.

2.3.5 Partial Randomization

The partial randomization method reconstructs a graph (say A) with partial rewirings with respect to a second graph (say B) while keeping the degree distribution the same

as in A. The analogy of this algorithm is to perform rewirings in the adjacency matrix of A, while avoiding any edge generation which already exist in the B. In other words, the choice of edges to be performed rewirings in A is limited with respect to the B.

In this project, the functional connectivity (FC) adjacency matrix is partially rewired with respect to the anatomical connectivity (AC) adjacency matrix. This means doing such rewirings among the nodes in FCM only if these nodes are not structurally connected in the brain with probability above a given value. The same procedure is done to randomize AC adjacency matrix partially with respect to FC adjacency matrix. This time nodes in ACM can be linked only if they are not functionally correlated above a given threshold.

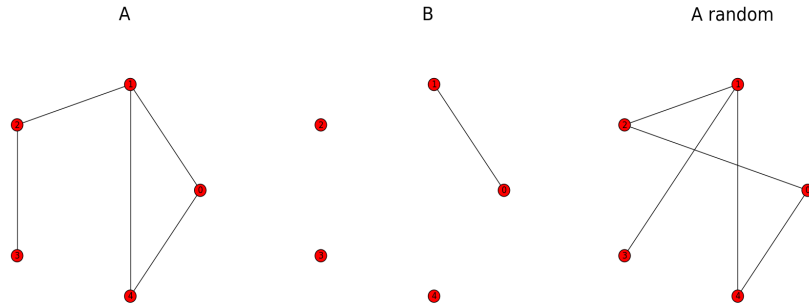


FIGURE 2.9: Graph A is performed a partial randomization with respect to graph B. While the partial randomization tool rewrites edges in A, it avoids creating such edges that exist in B.

Representative graphs *A* and *B* in Figure 2.9 can be thought as FCM and ACM, respectively. In this case, *A random* is the partially randomized graph of FCM with respect to ACM.

The brain graph and randomly generated graphs will be identified in terms of their topological properties in the following sections. For simplicity the abbreviations are introduced in the table below.

TABLE 2.1: Abbreviations for the brain graph and the randomly constructed graphs.

Abbreviation	Description	method
R0	the brain graph	NETWORKX
Ra	Erdős-Rényi, $G(N,L)$	NETWORKX
Rd	double-edge-swap	NETWORKX
Rh	preserved-degree-distribution	BCT
Rg	configuration model	NETWORKX
Rk	partial randomization	BCT

2.4 Network Characterizations

2.4.1 Network Density

The *average degree* $\langle k \rangle$ of a network is proportional to the ratio of total number of edges L to total number of nodes N in a graph,

$$\langle k \rangle = \frac{2L}{N}. \quad (2.2)$$

It should be noted that in order to not count each edge twice, the total number of edges is divided by $N/2$ instead of N . The *density* D of a network is a scaled version of average degree measurement. It is formulated as the ratio between L and maximum number of possible edges $\binom{N}{2}$,

$$D = \frac{2L}{N(N - 1)}. \quad (2.3)$$

The measure of network density can be referred to as the total *wiring cost* of the network [2]. The degree, average degree and network density are key scalar measures to characterize the topology of a network. There is for instance clinical evidence that reductions in nodal degree are associated with greater severity of local amyloid deposition in patients with Alzheimer's disease [17].

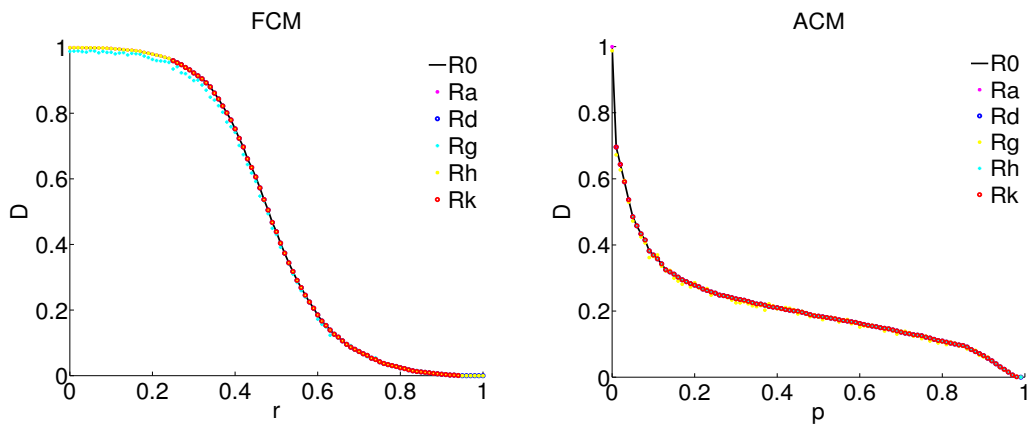


FIGURE 2.10: Network density of the brain graphs and random graphs of FCM (on the left) and ACM (on the right). The abbreviations are chosen as described in Table 1.

The network density D can be considered a probability for all graphs in corresponding threshold r and p ranges. The random networks are built in such ways that they have

the same number of nodes and almost the same D as in the brain graphs. However, the D is not a unique metric identifying a network.

All networks for FCM and ACM are densely connected for low r and p . For the brain graph and randomized graphs of FCM, D decreases sigmoidally with r . In comparison, D decreases slower with p for ACM graphs. It should be noted that all graphs have almost the same D values.

Functional networks are likely to be denser than anatomical networks, as they will typically contain numerous connections between anatomically unconnected regions [18].

2.4.2 Average Clustering Coefficient

The *average clustering coefficient* C of a network is calculated through individual clustering coefficients C_i of single nodes,

$$C = \frac{1}{n} \sum_{i \in N} C_i = \frac{1}{n} \sum_{i \in N} \frac{2t_i}{k_i(k_i - 1)}. \quad (2.4)$$

where t_i is the number of triangles around node i and k_i is the degree of node i [5]. The clustering coefficient is a measure of segregation, that is the ability for specialized processing to occur within densely interconnected groups of brain regions [2]. It reveals how the individual nodes in a graph cluster together; how many neighbors of a node are neighbors of each other.

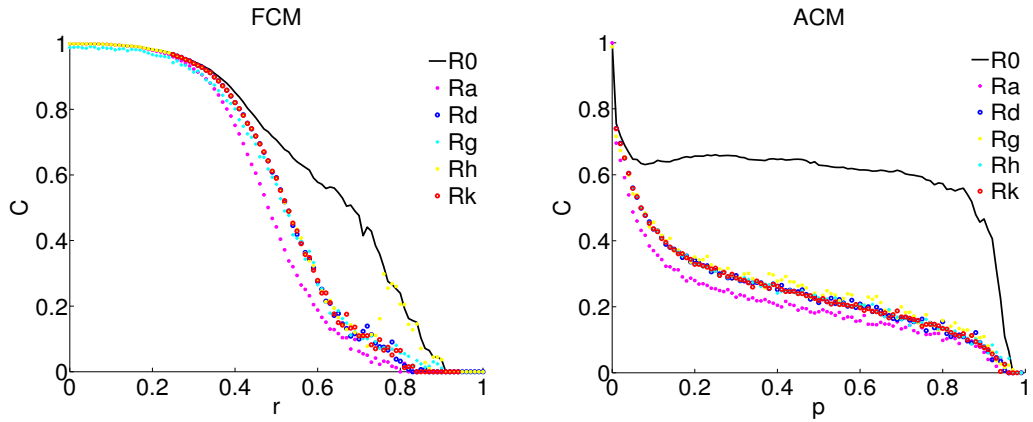


FIGURE 2.11: Average clustering coefficient of the brain graphs and random graphs of FCM (on the left) and ACM (on the right).

The clustering coefficient C_i of a node i is a measure of local connectivity and is highly correlated with the local efficiency of the information transfer [4]. The C_i is formulated as the ratio of t_i over all possible edges of the node i ; $\binom{k_i}{2}$. The average clustering

coefficient C is a normalized version of C_i for the whole network, yielding now a global property. All C values are between 0 and 1. Figure 2.7 shows that at lower binarization thresholds, nodes tend to cluster more due to higher number of existing edges. The empirically obtained brain networks of FCM and ACM have the highest C compared to random graphs. The local information transfer seems to be more efficient in the brain graphs. The randomized graphs of ACM Ra , Rd , Rh and Rk share more nodes with lower degrees compared to $R0$.

2.4.3 Transitivity

Transitivity is a similar measure to the clustering coefficient, and also quantifies segregation in the network. It is defined as [6]

$$T = \frac{\sum_{i \in N} 2t_i}{\sum_{i \in N} k_i(k_i - 1)}. \quad (2.5)$$

If a node has links to two other nodes, transitivity inquires whether those two other nodes are also connected to each other. It asks, what percentage of triangles in the network is closed. Transitivity resembles clustering coefficient, however, it is defined only for the whole network rather than single nodes.

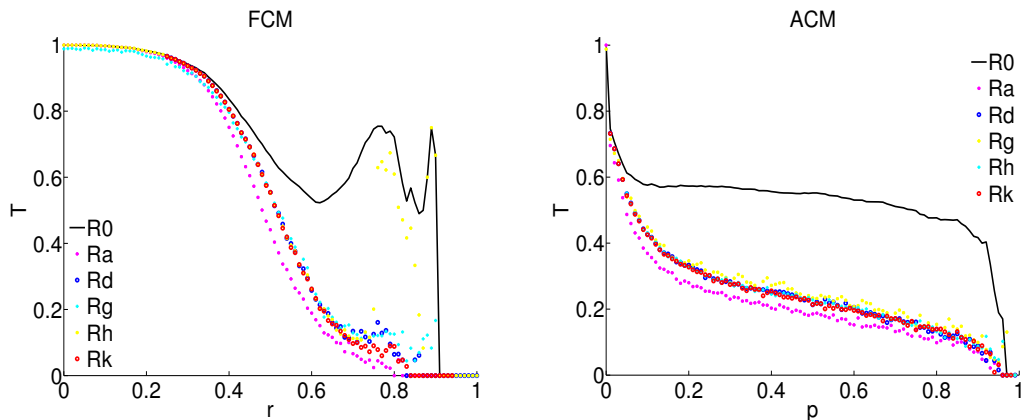


FIGURE 2.12: Transitivity of the brain graphs and random graphs of FCM (on the left) and ACM (on the left).

The degree of transitivity is one of the fundamental differences between real world networks and random networks [19]. This difference is more pronounced than the clustering difference between brain graphs and random graphs (see Figures 2.7 and 2.8). T is more effected with $P(k)$ of a network, the more nodes with lower degrees, the higher the T is. ACM related graphs tend to have lower $p(k')$ values distributed among many nodes,

whereas FCM related graphs have higher $p(k')$ values distributed among less nodes. This holds even for $R0$ and Rh graphs of FCM in Figure 2.12, that their $P(k)$ is reflected in higher T (see Appendix).

2.5 FitzHugh-Nagumo Model for Neuronal Activity Simulation

An fMRI-BOLD experiment reveals the correlation coefficients between timeseries of BOLD activity among pre-defined brain regions. The empirical functional connectivity matrix (FCM) derived from fMRI-BOLD technique in this project reflects those coefficients among $N = 90$ AAL regions at the resting state of human brain, i.e. no stimulus driving approach is introduced to the subject. Despite lack of any stimulus, the observed fMRI-BOLD signal in the mammalian brain is highly structural and robust at low frequency fluctuations (<0.1 Hz) [20–22]. However, the underlying reason of these well organized spatio-temporal dynamics has not yet been completely resolved. The existing models of resting-brain dynamics hypothesize that functional interactions result from a complex interplay between intrinsic brain dynamics and anatomical connections [9]. This section proposes a modeling approach for the ongoing neuronal activity at brain's resting state, i.e. how underlying correlated behavior among distant cortical brain regions arise [23]. Once the model is fulfilled with bio-physically plausible parameter ranges with the help of previous studies, the timeseries of nodes in brain graphs will be extracted by means of model simulations as well as in randomly constructed networks.

The theoretical model of choice for the neuronal activity is FitzHugh-Nagumo (FHN) systems describing physiological states of nerve membrane potential [24, 25]. FHN model will be used to represent the neuronal activity of a nerve cell population, in other words, an AAL node in this project. Local dynamics of a single node will then be globalized in the whole brain network via mutual time delayed interactions among nodes. Here, time delay $\delta\tau_{ij}$ is assumed to arise from a limited signal propagation velocity v between nodes i and j , furthermore, time delayed interactions are scaled with a coupling strength c [26–28]. Another important parameter for FHN simulations is threshold r or probability p values used to extract adjacency matrices from FCM and ACM. The first objective is to investigate such plausible c , v , and r or p ranges at which our simulated neuronal activity of brain graphs are similar to the empirical fMRI-BOLD data.

FHN model will also be applied on randomly constructed graphs described in the previous section. The second objective is to identify such regions in the explored parameter

space for which the simulated timeseries of the empirically obtained networks are distinguishable than that of randomly constructed graphs. The effects of c , v , r or p as well as network characteristics of graphs will be taken into consideration. At the end, it is aimed to gain further insight into the key features of anatomical brain structures by comparing to randomized networks.

The FHN model is designed to reflect the neuronal activity as simulated timeseries, it is not corresponding the BOLD activity. The comparison of simulated BOLD activity to the fMRI-BOLD signal would be ahead of timeseries comparison approach. The last objective of FHN model is the following: the simulated neuronal activity will be finally used to infer the BOLD signal via the Balloon-Windkessel hemodynamic model in the last section [29].

Subsections will describe set of non-linear differential equations for the FHN local dynamics and carry out a stability analysis. Dynamics of a single node will then be globalized via mutual couplings with a second node and the effect of time delay interactions will be demonstrated. The last part will embed complete FHN simulation to a simple graph and the first exemplary timeseries of a node will be illustrated.

2.5.1 FHN Model Local Dynamics

This section aims to demonstrate local dynamics of a brain node with FHN model. Here, the node is assumed to be isolated, meaning that it is not connected to any other node at all in the brain. FHN model has an activator variable x and an inhibitor variable y , their time evolution is represented with the same implementation as in [26, 27] in following non-linear differential equations,

$$\dot{x} = \tau(y + \gamma x - \frac{x^3}{3}) \quad (2.6a)$$

$$\dot{y} = -\frac{1}{\tau}(x - \alpha + by - I) \quad (2.6b)$$

where τ denotes the time constant accelerating x , I is the external stimulus parameter and γ , α , b are other system parameters. x and y are considered to be counteracting variables capturing membranous potential alterations on a neuronal population around 10^9 cells. Non of the activator or the inhibitor variables includes any coupling parameter for the described local activity and additionally I is chosen to be 0 [26].

The *fixed point* (x_f, y_f) of the system is defined such that there is no change in variables over time $\dot{y} = \dot{x} = 0$. The fixed point condition substituted back into equations (2.6a)

abd (2.b6) yields set of *nullcline* equations,

$$y = \frac{x^3}{3} - \gamma x \quad (2.7a)$$

$$x = \alpha - by \quad (2.7b)$$

where equation (2.7a) will be called as y -*nullcline* and (2.7b) as x -*nullcline* from now on. The stability analysis is performed by calculating eigenvalues of the *Jacobian Matrix*, \mathbf{J} at the intersection of nullclines, (x_f, y_f) . The linearization of equations (2.6a) and (2.6b) helps to find \mathbf{J} straightforward,

$$\begin{pmatrix} \frac{dx}{dt} \\ \frac{dy}{dt} \end{pmatrix} = \begin{pmatrix} \tau(\gamma - x_f^2) & \tau \\ -\frac{1}{\tau} & -\frac{b}{\tau} \end{pmatrix} \begin{pmatrix} x \\ y \end{pmatrix} \quad (2.8)$$

where,

$$\mathbf{J} = \begin{pmatrix} \tau(\gamma - x_f^2) & \tau \\ -\frac{1}{\tau} & -\frac{b}{\tau} \end{pmatrix} \quad (2.9a)$$

$$\det \mathbf{J} = b(x_f^2 - \gamma) + 1 \quad (2.9b)$$

$$\text{tr} \mathbf{J} = \frac{1}{\tau}(\tau^2(\gamma - x_f^2) - b) \quad (2.9c)$$

Eigenvalues of \mathbf{J} are calculated as the following,

$$\det(\mathbf{J} - \lambda \mathbf{I}) = 0 \quad (2.10a)$$

$$\lambda^2 - \lambda \text{tr} \mathbf{J} + \det \mathbf{J} = 0 \quad (2.10b)$$

$$\lambda_{1,2} = \frac{\text{tr} \mathbf{J} \pm \sqrt{\text{tr}^2 \mathbf{J} - 4 \det \mathbf{J}}}{2} \quad (2.10c)$$

$$\lambda_{1,2} = \frac{\tau^2(\gamma - x_f^2) - b \pm \sqrt{(\tau^2(x_f^2 - \gamma) - b)^2 - 4\tau^2}}{2\tau} \quad (2.10d)$$

Parameters in FHN model are tuned so that solutions would render a damped oscillatory behavior for each node locally; $\alpha = 0.85$, $b = 0.2$, $\gamma = 1.0$ and $\tau = 1.25$ [23]. The solution of the condition $\dot{y} = \dot{x} = 0$ gives coordinates of $(x_f, y_f) = (0.98, -0.67)$, which is calculated numerically here. All parameters plugged in eigenvalue equation (2.10d) results in $\lambda_1 = -0.056 + 0.996i$ and $\lambda_2 = -0.056 - 0.996i$. Since real parts of both eigenvalues stand below zero, the fixed point is said to be *stable*. λ_1 and λ_2 are complex conjugate pairs, the fixed point can be alternatively called as a *stable focus*. Variables x and y are expected to relax onto the fixed point over time.

The time evolution of x and y resembles damped oscillations at the beginning. Following to a rapid excitation and inhibition, both variables converge to the fixed point. State

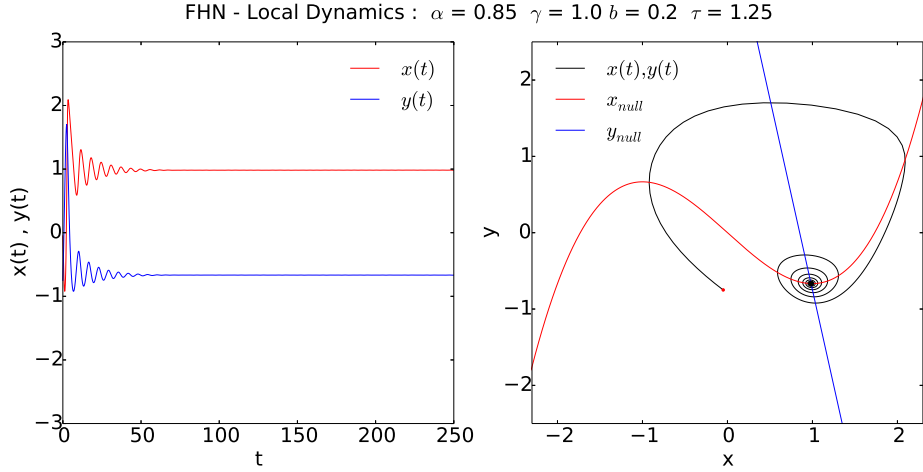


FIGURE 2.13: Local dynamics of an isolated node: time evolution of x and y (on the left) and nullclines on state space together with $x(t), y(t)$ (on the right). The fixed point $(x_f, y_f) = (0.98, -0.67)$ is drawn with a black dot at the intersection of nullclines and initial point (x_0, y_0) is illustrated with a red dot.

space illustrates this relaxation over nullclines, a clockwise trajectory starting from a randomly chosen (x_0, y_0) and falling on (x_f, y_f) with smaller and smaller amplitude oscillations. The system is in quiescent state, but can also be said to be at the onset of instability. The scale of change in x is more pronounced than y due to τ proportionality in the definition of \dot{x} in FHN model.

2.5.2 Noise Effect

The local dynamics of a node can be extended with an additional noise factor,

$$\dot{x} = \tau(y + \gamma x - \frac{x^3}{3}) + Dn_x \quad (2.11a)$$

$$\dot{y} = -\frac{1}{\tau}(x - \alpha + by - I) + Dn_y \quad (2.11b)$$

where D is the noise strength, n_x and n_y represent Gaussian white noises. Neither coordinates of the fixed point or eigenvalues are affected due to the noise factor. However, dynamics of the system is forced to go under a change such that the stability will be lost.

The noise drives sub-threshold oscillations as realized in the time evolution of activator and inhibitor. It prevents x and y variables from relaxing on the fixed point, instead, they fluctuate around it. This dynamics remarks the onset of instability, and it is called "type II excitation" in terms of neuronal dynamics.

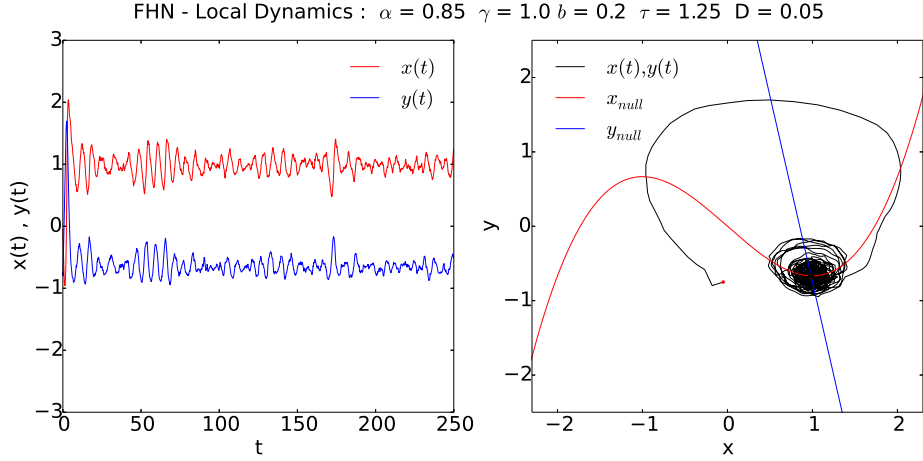


FIGURE 2.14: Local dynamics of two variables x and y with same parameters as previously stated, an additional Gaussian white noise with strength $D = 0.05$ is added. The fixed point $(x_f, y_f) = (0.98, -0.67)$ is drawn with a black dot in state space where two nullclines intersect.

2.5.3 Global Dynamics

This section demonstrates the effect of mutual coupling between two exemplary nodes with FHN model. Now, we consider two nodes connected to each other, either functionally or structurally as in FCM or in ACM. The effect of this connection is captured theoretically with a global coupling term and time delayed interactions,

$$\dot{x}_1 = \tau(y_1 + \gamma x_1 - \frac{x_1^3}{3}) + C[x_2(t - \tau_{12})] + Dn_{x1} \quad (2.12a)$$

$$\dot{y}_1 = -\frac{1}{\tau}(x_1 - \alpha + by_1 - I) + Dn_{y1} \quad (2.12b)$$

$$\dot{x}_2 = \tau(y_2 + \gamma x_2 - \frac{x_2^3}{3}) + C[x_1(t - \tau_{21})] + Dn_{x2} \quad (2.12c)$$

$$\dot{y}_2 = -\frac{1}{\tau}(x_2 - \alpha + by_2 - I) + Dn_{y2} \quad (2.12d)$$

where C is the coupling strength, subindices 1 and 2 stand for corresponding nodes, τ_{12} and τ_{21} are time delays required for coupled node interactions and D is the Gaussian white noise strength. For simplicity, the global dynamics are illustrated with same local parameters as before, while time delays are taken to be homogeneous, $\tau_{12} = \tau_{21} = 0.5$.

The mutual coupling between nodes pushes both systems (x_1, y_1) and (x_2, y_2) to be oscillatory with visibly larger amplitudes in comparison to local dynamics and noise effect in previous figures. The system does not fall on to the fixed point anymore, indicating loss of the stability.

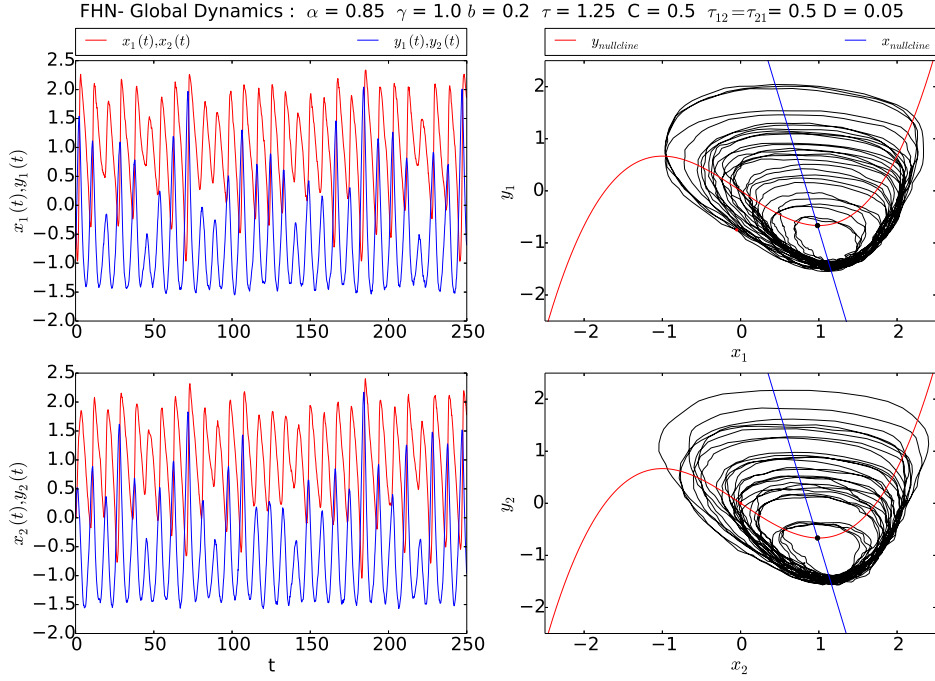


FIGURE 2.15: Global dynamics of two nodes with variables x_1, y_1 and x_2, y_2 . The fixed point is the same for both systems $(x_f, y_f) = (0.98, -0.67)$, it is drawn with a black dot at the intersection of nullclines in state space.

2.5.4 FHN Time Series

After introducing the local and global dynamical models of nodes, the final version of FHN model to be simulated as the neuronal activity in the complete brain graph or random network is denoted with the following notation [23],

$$\dot{x}_i = \tau(y_i + \gamma x_i - \frac{x_i^3}{3}) - c \sum_{j=1}^N a_{ij} x_j(t - \Delta t_{ij}) + D n_x \quad (2.13a)$$

$$\dot{y}_i = -\frac{1}{\tau}(x_i - \alpha + b y_i - I) + D n_y \quad (2.13b)$$

where the index i represents any node among $N = 90$ AAL regions, c is coupling strength, a_{ij} is corresponding connectivity unit between nodes i and j in adjacency matrix. This is the crucial link between network analysis part and FHN section. If nodes are connected in a given network, then $a_{ij} = 1$, otherwise $a_{ij} = 0$. Δt_{ij} is the time delay factor arising from finite signal propagation velocity v among nodes. Δt_{ij} is calculated as $\Delta t_{ij} = \frac{d_{ij}}{v}$ [26–28], where d_{ij} is the matrix of Euclidean distances between centers of brain regions from which BOLD time series are extracted [30]. The external stimulus is again set

to zero $I = 0$. The noise (n_x, n_y) factors are Gaussian white noise distributions, the strength of noise is $D = 0.05$, large noise.

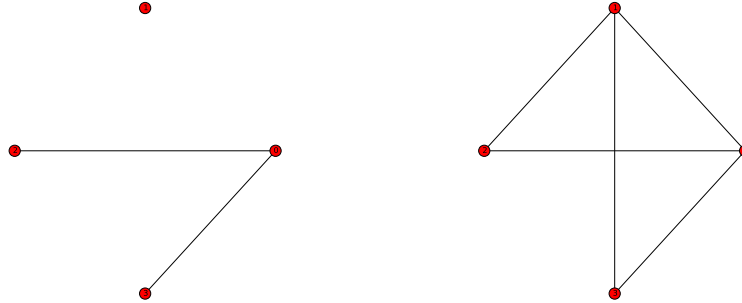


FIGURE 2.16: Two sample graphs to be simulated with FHN model, the upper-most node, say node 1 is not connected at all in first graph (on the left) and connected by 3 edges in second graph (on the right).

The time delay coupled set of ordinary differential equations is solved numerically with PYTHON-module PYDELAY-algorithm based on Bogacki-Sampine method [31, 32].

FHN timeseries of node 1, having no edge connections in first graph, is oscillatory, but the scale of oscillations seem to be small. Its dynamical view is in agreement with FHN local dynamics with noise effect. However, when node 1 is connected to 3 other nodes in second graph, then large scaled oscillatory patterns of its activator and inhibitor variables can be observed as a consequence of global coupling terms.

This section proposed to describe the chosen theoretical model for the neuronal activity. The next step is to study the introduced neuronal dynamics on empirically derived and randomly constructed graphs. $N = 90$ nodes in any given network will be simulated with the complete FHN timseries notation for 7.5 minutes. Then, Pearson correlation coefficients between simulated timeseries of node pairs will be calculated for one graph. A 90×90 correlation matrix will raise for each FHN simulated network.

FHN model is involved in crucial steps in this Master's project: parameter analysis, distinguishing brain graphs and random graphs and finally extracting BOLD activity. Simulations on brain graphs obtained from FCM and ACM matrices will be compared to the original fMRI-BOLD data in parameter spaces by tuning three parameters in bio-physically plausible ranges: coupling strength c and velocity v as well as a threshold r or probability p value, which is used while constructing adjacency matrices a_{ij} of given

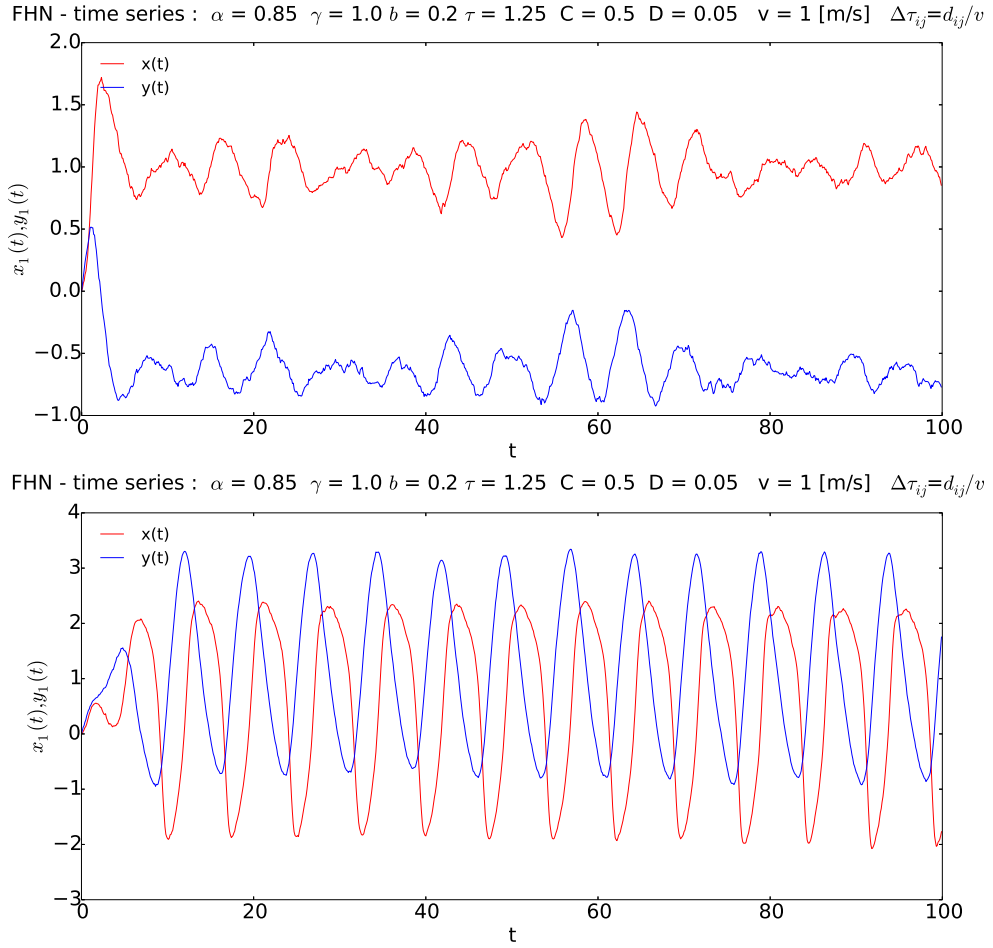


FIGURE 2.17: Analogous time series of node 1 chosen from graphs illustrated in previous figure. Timeseries at top is of the unconnected node, at down is of 3-edge connected node. All parameters besides d_{ij} matrix are chosen to be biologically plausible. An unrealistic d_{ij} is filled out for corresponding sample graphs in previous figure.

graphs. Simulations on random graphs will be used to identify regions in the explored parameter space for which the empirical data differ from that of the random graphs. Not only the effect of tuned parameters c , v and r or p , but also the contribution of topological measurements of graphs will be taken into account. At the end, FHN timeseries of brain graphs will be simulated further with another theoretical model to capture the BOLD signal, which will be introduced in the next session.

2.6 Balloon-Windkessel Model for BOLD Activity Simulation

Blood oxygen level dependent (BOLD) effect is one of the underlying contrast mechanisms of fMRI to map brain activity at resting state. BOLD signal is thought to arise

from interactions between neuronal activity and regional changes in the surrounding of those active neurons such as blood volume, blood flow and oxygenation level in capillaries. When neuronal activity increases, the blood flow in blood vessels surrounding this neuronal region rises, causing a change in relative amounts of deoxygenated and oxygenated forms of Hemoglobin (dHB and Hb). The difference in magnetic properties of dHB (paramagnetic) and Hb (diamagnetic) is the key ingredient to the observed changes in magnetic resonance signal. A better understanding of the resting state BOLD signal is required to better interpret neuronal activity. The previous section proposed already a model for the neuronal activity, FHN model. This section will introduce a hemodynamic process to capture BOLD activity with a mathematical model known as Balloon model [33].

In addition to the variations in magnetic properties of the blood caused by blood flow in vessels, there are other physiological changes during alteration in neuronal activity that affect the temporal dynamics of BOLD signal, i.e. cerebral blood flow (CBF), cerebral blood volume (CBV), cerebral metabolic rate of oxygen consumption ($CMRO_2$). Moreover, the BOLD response is subject dependent: the physiological baseline state of the individual under examination is used to scale BOLD response and this fact brings another difficulty to interpret the BOLD signal, when the baseline state varies [34]. The sensitivity of BOLD signal to the variations in vascular and metabolic physiology brings a great complexity to interpret it accurately. The biophysical descriptions of the BOLD signal are still not fully satisfactory for the resting state.

Changes in the BOLD signal obtained in an fMRI experiment represent an indirect measure of underlying neuronal activity [11]. The modeled neuronal activity can be used to infer the BOLD signal observed in the fMRI data via Balloon-Windkessel hemodynamic process, which mediates between a non-linear timeseries and measured BOLD response [29]. In short, the Balloon-Windkessel model picks an input signal from neuronal activity timeseries and turnouts the BOLD activity timeseries as a function of changes in CBF, CBV, $CMRO_2$. The main input of Balloon-Windkessel model is a neuronal signal in the form of either a spiking rate or a local field potential [35]. The neuronal signal in this project will be normalized FHN timeseries of activator variable, which describes the excitatory membrane potential dynamics of a neuronal population.

The study of Friston et al. shows that it is possible to capture ultra-slow frequency oscillations (< 0.1) in the hemodynamic process, given a higher frequency neuronal input for event related responses [29]. Here, the same model will be tested for the resting state activity to find out whether it is possible to extract BOLD activity from FHN modeled $N = 90$ AAL brain nodes. Each brain graph obtained from FCM and ACM data sets will be embedded into Balloon-Windkessel model, and a new parameter analysis will be

carried out while comparing resultant BOLD simulations to the fMRI-BOLD empirical data set.

2.6.1 Hemodynamic Model

This section is designed to review the Ballon-Windkessel hemodynamic model explained in Friston et al [29].

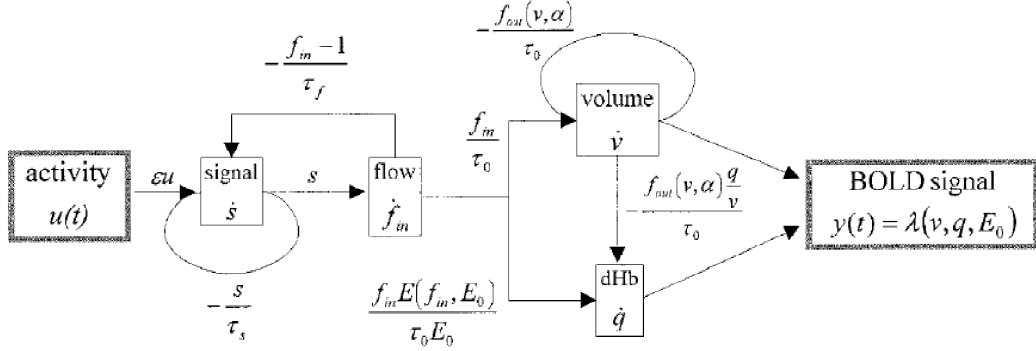


FIGURE 2.18: The hemodynamic model for the BOLD activity illustrated in Friston et al. [29]

TABLE 2.2: Notations and their brief descriptions for hemodynamics in Friston et al.

Abbreviation	Description
$u(t)$	nonlinear input signal
s	blood flow inducing signal
τ_s	time constant to describe \dot{s}
f_{in}	CBF (inflow)
τ_f	feedback time constant
v	CBV
τ_0	mean transit time \dot{v}
α	stiffness exponent
$f_{out}(v, \alpha)$	CBF (outflow)
E_0	resting net O_2 extraction rate
$E(f_{in}, E_0)$	fraction of O_2 extracted from f_{in}
q	dHb content in voxel
$y(t)$	output BOLD signal

The CBF is denoted by two symbols based on its flow direction: f_{in} and f_{out} , venous blood inflow and outflow, respectively. The nonlinear neuronal activity $u(t)$ and f_{in} are thought to accomplish the blood flow inducing signal s . Equation (2.14a) represents time dependent change of this signal \dot{s} depending on $u(t)$, f_{in} and s . Three system parameters ϵ , τ_s and τ_f are described as following: an efficacy parameter for $u(t)$ to

raise up s , a time constant for s decay, and another time constant for autoregulatory feedback from CBF [36, 37].

Hemodynamics in brain assumes that alterations in regional CBF is shaped by an underlying neuronal activity. Equation (2.14b) presents the rate of change of f_{in} with a linear transformation on s , which can originate from a nonlinear neuronal activity model [38, 39].

The alteration in cerebral blood volume \dot{v} is basically formulated by subtracting f_{out} from f_{in} , both rated physiologically with a time constant τ_0 , which is also referred as *mean transit time* [40]. The Windkessel model contributes to the brain hemodynamics while modeling CBF through CBV: equation (2.15a) describes a function for f_{out} depending on v and a parameter α , namely *stiffness exponent* [40].

The change in magnetic properties of blood is expressed with the difference between dHb uptake and release. dHb uptake is proportional to the blood inflow f_{in} to the venous compartment and available O_2 to be coupled to Hb. The amount of O_2 carried with blood inflow is estimated with a function $E(f_{in}, E_0)$ divided by resting net O_2 extraction rate E_0 as given in equation (2.15b) [33]. dHb release is proportional to the blood outflow f_{out} and the concentration of dHb in corresponding voxel volume v .

$$\dot{s} = \epsilon u(t) - \frac{s}{\tau_s} - \frac{f_{in} - 1}{\tau_f} \quad (2.14a)$$

$$\dot{f}_{in} = s \quad (2.14b)$$

$$\dot{v} = \frac{f_{in}}{\tau_0} - \frac{f_{out}(v, \alpha)}{\tau_0} \quad (2.14c)$$

$$\dot{q} = \frac{f_{in}E(f_{in}, E_0)}{\tau_0 E_0} - \frac{f_{out}(v, \alpha) q}{\tau_0} \frac{q}{v} \quad (2.14d)$$

$$f_{out}(v, \alpha) = v^{1/\alpha} \quad (2.15a)$$

$$E(f_{in}, E_0) = 1 - (1 - E_0)^{1/f_{in}} \quad (2.15b)$$

Finally, the output BOLD signal is modeled as a function depending on variables v , q and parameter E_0 ,

$$y(t) = \lambda(v, q, E_0) = V_0(k_1(1 - q) + k_2(1 - \frac{q}{v}) + k_3(1 - v))) \quad (2.16)$$

where $k_1 = 7E_0$, $k_2 = 2$ and $k_3 = 2E_0 - 0.2$, V_0 is resting blood volume fraction. The set of differential equations for \dot{s} , \dot{f}_{in} , \dot{v} , \dot{q} are all solved with simple Euler's method algorithm with step size $dt = 0.001$ numerically. The six unknown parameters ϵ , α , τ_0 , τ_f , τ_s and E_0 are picked up from proper ranges given in Friston et al.

Chapter 3

Results

3.1 FHN

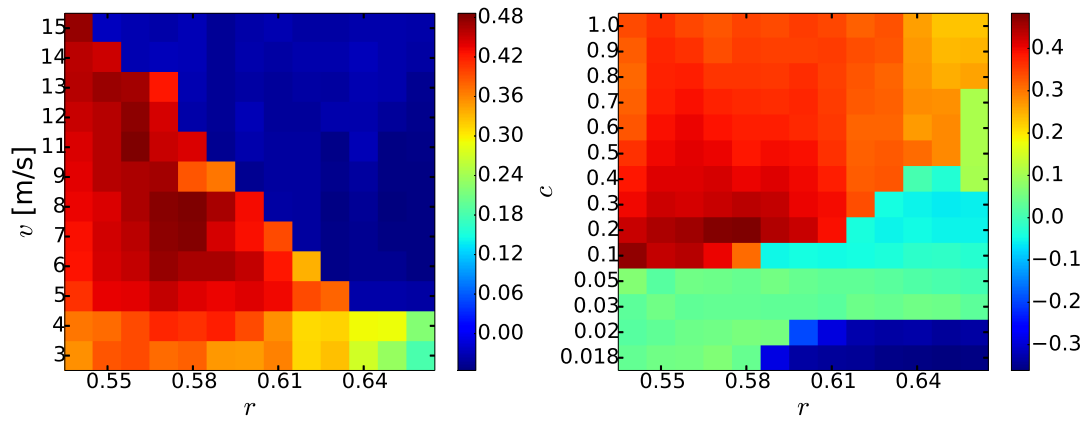


FIGURE 3.1: FHN simulated FCM brain graphs, parameter analysis, $v = 7[m/s]$ on the left and $c = 0.2$ on the right

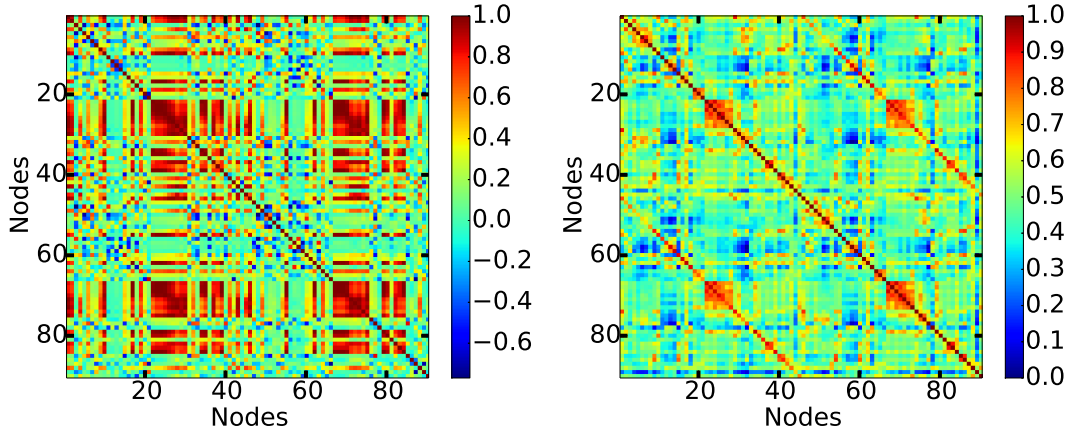


FIGURE 3.2: Best correlated FHN simulation of FCM brain graph with $c = 0.2$, $v = 7[m/s]$ and $r = 0.60$ (on the left) and empirical FCM obtained from fMRI-BOLD.
 $\rho_{e,s} = 0.43$

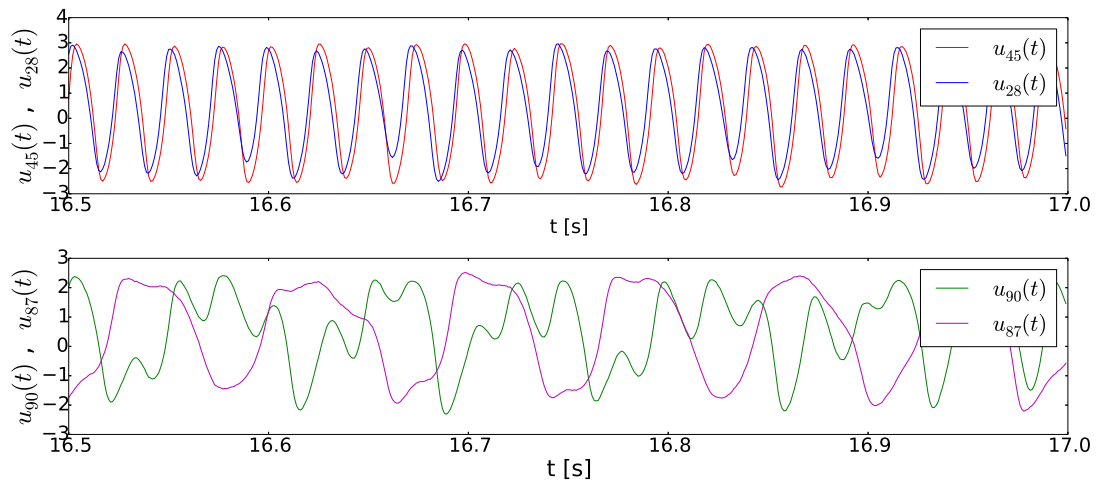


FIGURE 3.3: Simulated neuronal activity of highly (at top, $\rho_{45,28} = 0.88$) and poorly (at bottom, $\rho_{90,87} = 0.13$) correlated node couples. Both nodes are chosen from the simulated correlation matrix of FCM in previous figure ($c = 0.2$, $v = 7[m/s]$, $r = 0.60$).

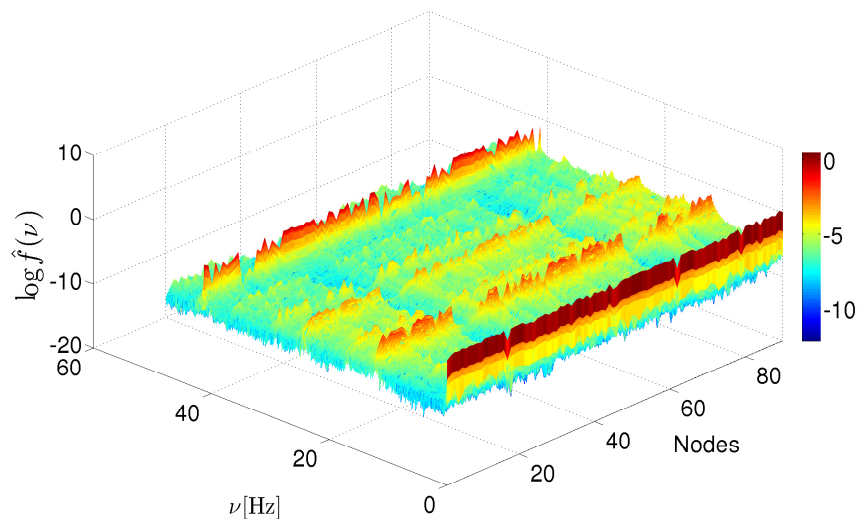


FIGURE 3.4: 3D illustration of fast fourier transform of neuronal activity oscillations corresponding to $N = 90$ nodes in FCM simulation with parameters given in Fig.3.2.

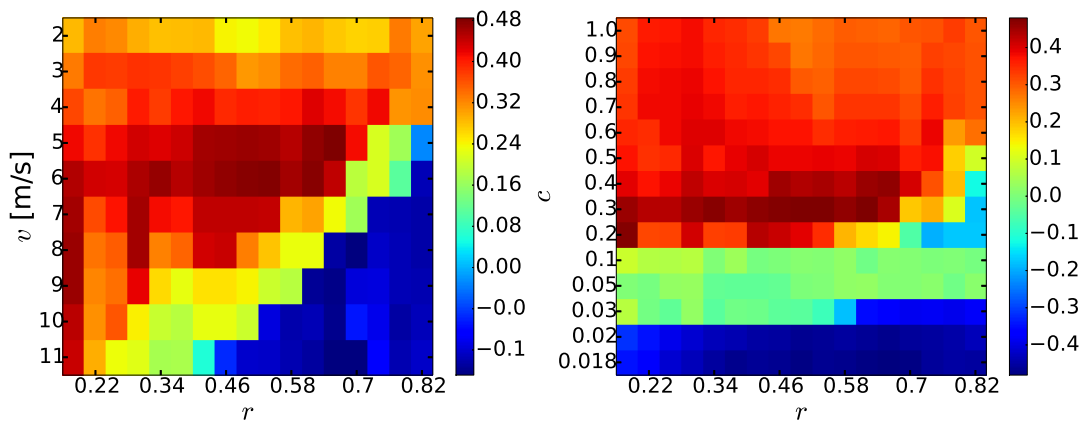


FIGURE 3.5: FHN simulated ACM brain graphs, parameter analysis, $v = 6[\text{m/s}]$ on the left and $c = 0.3$ on the right

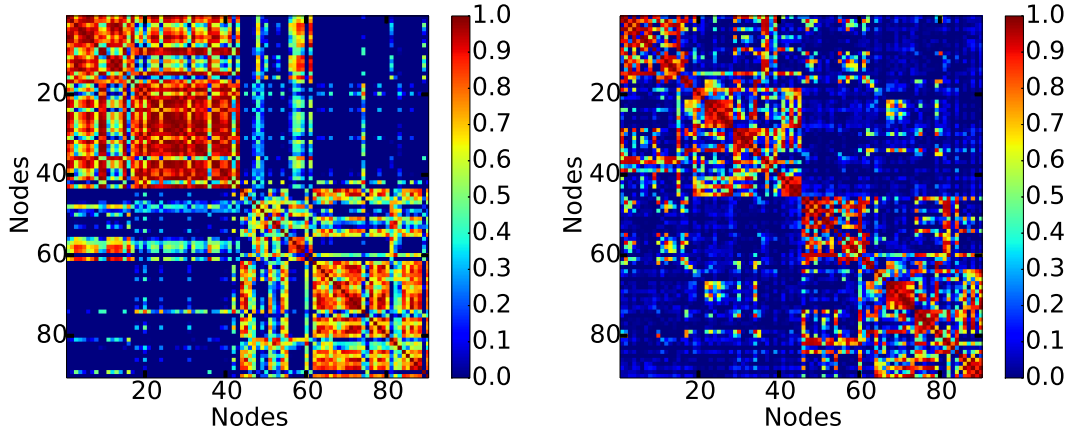


FIGURE 3.6: Best correlated FHN simulation of ACM brain graph with $c = 0.3$, $v = 6[m/s]$ and $r = 0.50$ (on the left) and empirical ACM obtained from DW-MRI.
 $\rho_{e,s} = 0.43$

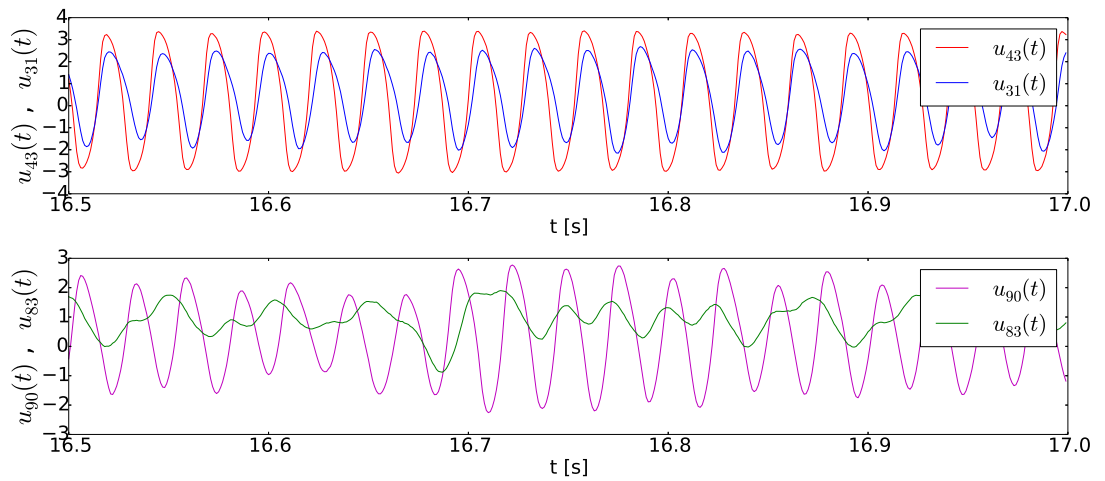


FIGURE 3.7: Simulated neuronal activity of highly (at top, $\rho_{43,31} = 0.86$) and poorly (at bottom, $\rho_{90,83} = 0.15$) correlated node couples. Both nodes are chosen from the simulated correlation matrix of ACM in previous figure ($c = 0.3$, $v = 6[m/s]$, $r = 0.50$).

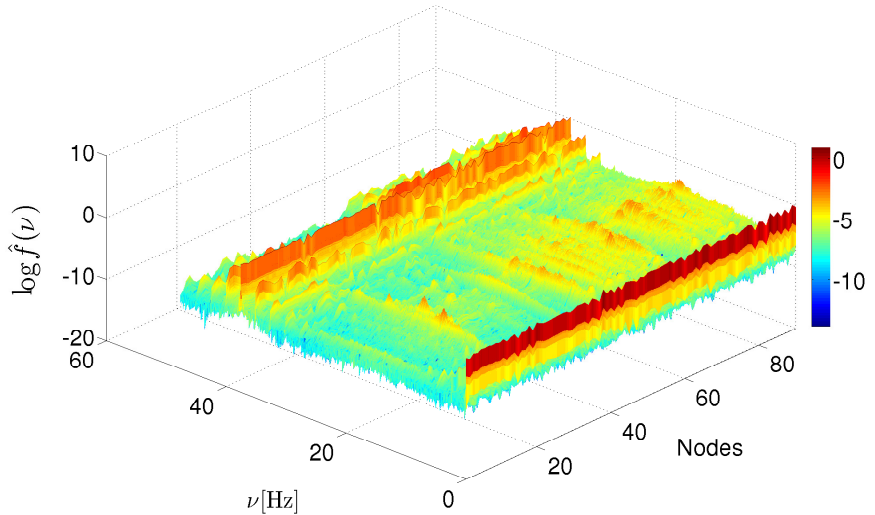


FIGURE 3.8: 3D illustration of fast fourier transform of neuronal activity oscillations corresponding to $N = 90$ nodes in ACM simulation with parameters given in Fig.3.6.

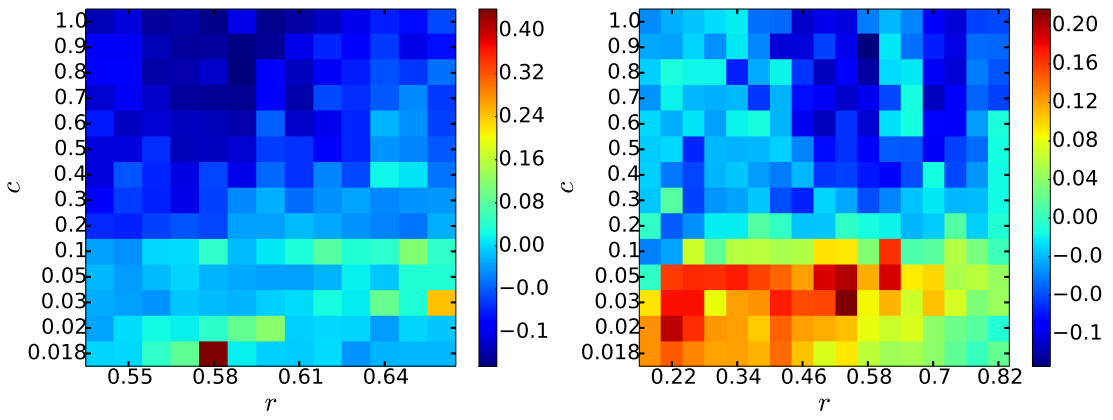


FIGURE 3.9: Parameter analysis for BOLD simulations done with FCM (on the left, $v = 7[m/s]$) and ACM (on the right, $v = 3[m/s]$). Note that both simulation outcomes are correlated with only empirical FCM.

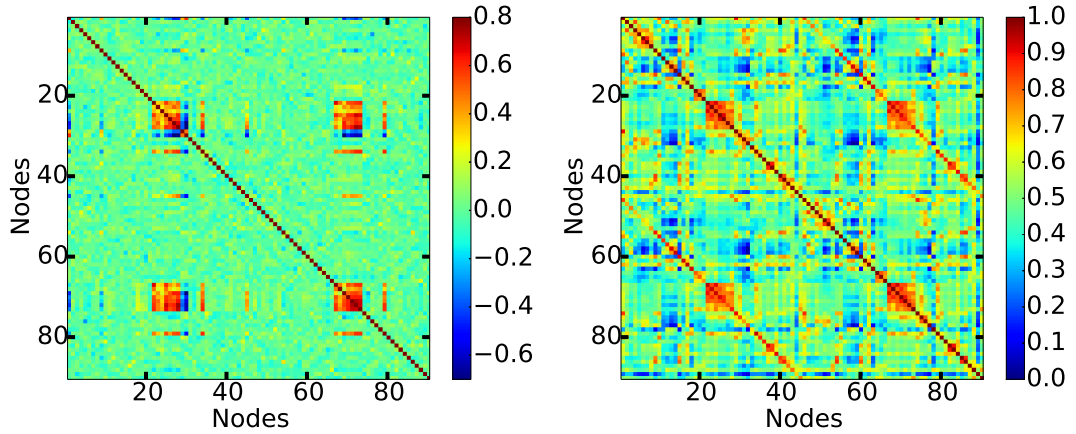


FIGURE 3.10: Highly correlated BOLD simulation of FCM brain graph with $c = 0.03$, $v = 7[m/s]$ and $r = 0.66$ (on the left) and empirical FCM obtained from fMRI-BOLD.
 $\rho_{e,s} = 0.24$

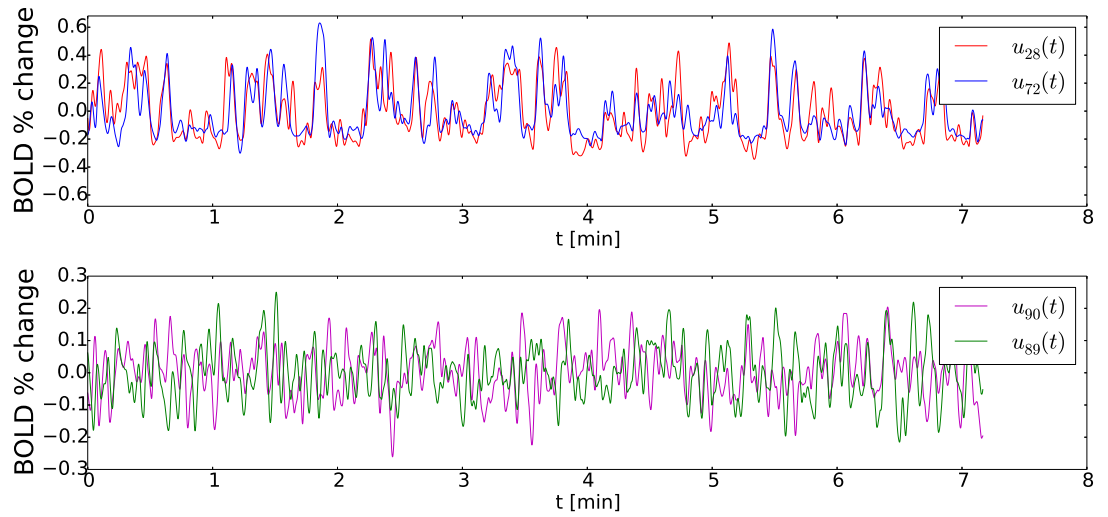


FIGURE 3.11: Simulated BOLD activity of highly (at top, $\rho_{28,72} = 0.75$) and poorly (at bottom, $\rho_{90,81} = 0.11$) correlated node couples. Both nodes are chosen from the simulated correlation matrix in previous figure ($c = 0.03$, $v = 7[m/s]$, $r = 0.66$).

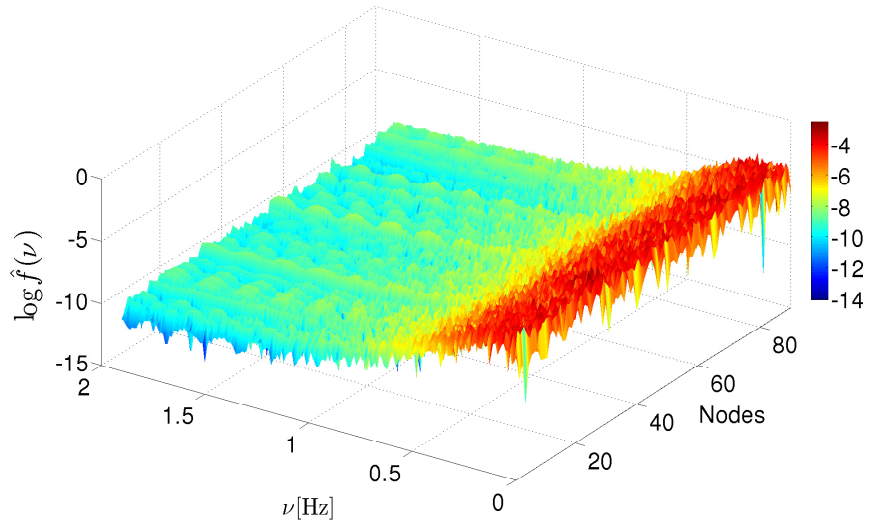


FIGURE 3.12: 3D illustration of fast fourier transform of BOLD activity slow oscillations corresponding to $N = 90$ nodes in FCM simulation with parameters given in Fig.3.10.

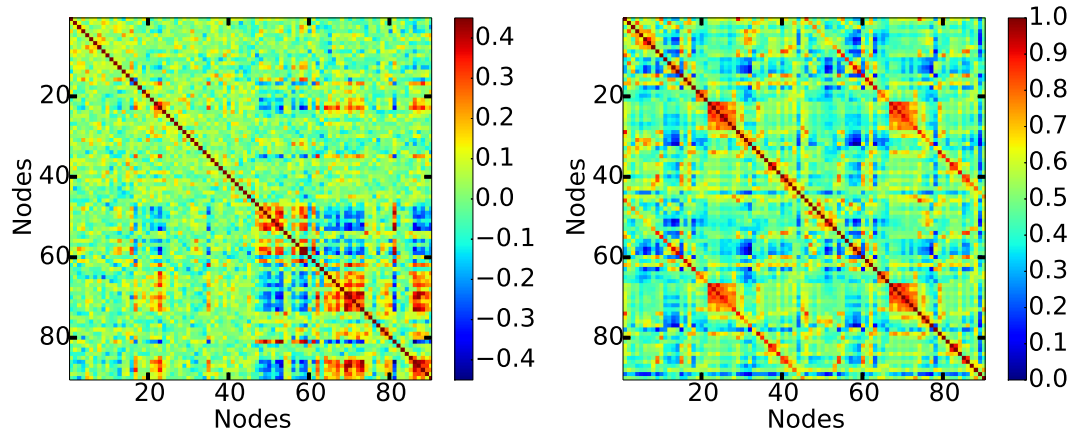


FIGURE 3.13: Highly correlated BOLD simulation of ACM brain graph with $c = 0.03$, $v = 3[m/s]$ and $r = 0.54$ (on the left) and empirical FCM obtained from fMRI-BOLD. $\rho_{e,s} = 0.22$

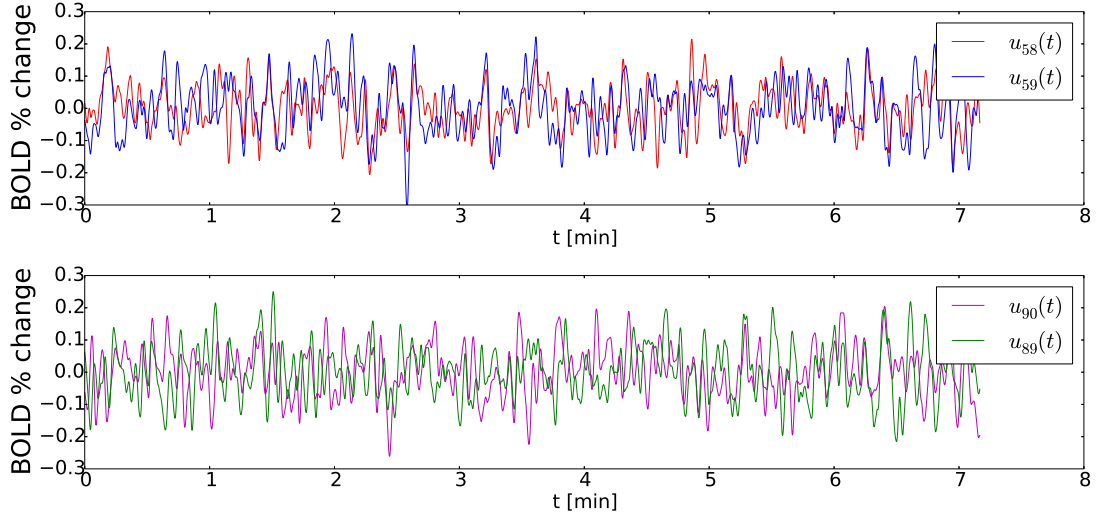


FIGURE 3.14: Simulated BOLD activity of highly (at top, $\rho_{58,59} = 0.48$) and poorly (at bottom, $\rho_{90,89} = 0.11$) correlated node couples. Both nodes are chosen from the simulated ACM correlation matrix in previous figure ($c = 0.03$, $v = 3[m/s]$, $r = 0.54$).

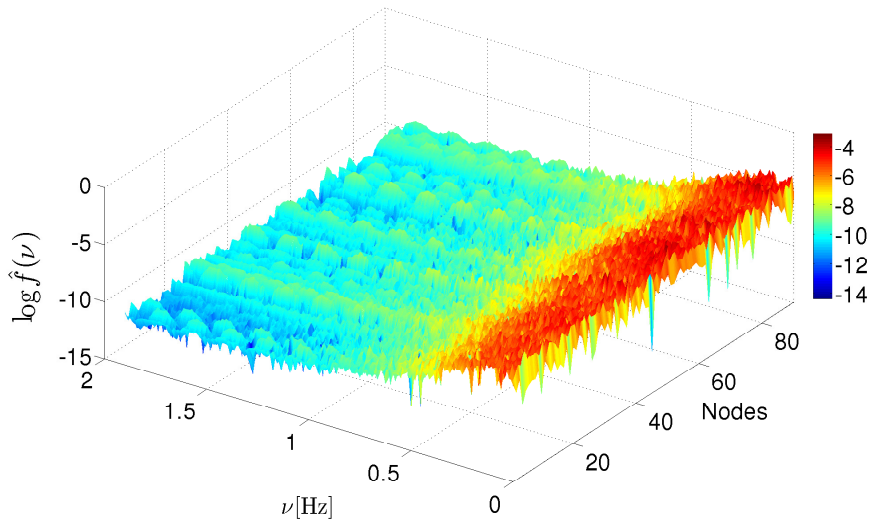


FIGURE 3.15: 3D illustration of fast fourier transform of BOLD activity slow oscillations corresponding to $N = 90$ nodes in ACM simulation with parameters given in Fig.3.13.

Chapter 4

Conclusion

4.0.1 Common L^AT_EX Math Symbols

There are a multitude of mathematical symbols available for L^AT_EX and it would take a great effort to learn the commands for them all. The most common ones you are likely to use are shown on this page:

<http://www.sunilpatel.co.uk/latexsymbols.html>

You can use this page as a reference or crib sheet, the symbols are rendered as large, high quality images so you can quickly find the L^AT_EX command for the symbol you need.

4.1 Getting Started with this Template

If you are familiar with L^AT_EX, then you can familiarise yourself with the contents of the Zip file and the directory structure and then place your own information into the ‘`Thesis.cls`’ file. Section 4.3 on page 41 tells you how to do this. Make sure you read section 4.5 about thesis conventions to get the most out of this template and then get started with the ‘`Thesis.tex`’ file straightaway.

If you are new to L^AT_EX it is recommended that you carry on reading through the rest of the information in this document.

4.1.1 About this Template

This L^AT_EX Thesis Template is originally based and created around a L^AT_EX style file created by Steve R. Gunn from the University of Southampton (UK), department of Electronics and Computer Science. You can find his original thesis style file at his site, here:

<http://www.ecs.soton.ac.uk/~srg/softwaretools/document/templates/>

My thesis originally used the ‘`ecsthesis.cls`’ from his list of styles. However, I knew L^AT_EX could still format better. To get the look I wanted, I modified his style and also created a skeleton framework and folder structure to place the thesis files in.

This Thesis Template consists of that modified style, the framework and the folder structure. All the work that has gone into the preparation and groundwork means that all you have to bother about is the writing.

Before you begin using this template you should ensure that its style complies with the thesis style guidelines imposed by your institution. In most cases this template style and layout will be suitable. If it is not, it may only require a small change to bring the template in line with your institution’s recommendations.

4.2 What this Template Includes

4.2.1 Folders

This template comes as a single Zip file that expands out to many files and folders. The folder names are mostly self-explanatory:

Appendices – this is the folder where you put the appendices. Each appendix should go into its own separate ‘`.tex`’ file. A template is included in the directory.

Chapters – this is the folder where you put the thesis chapters. A thesis usually has about seven chapters, though there is no hard rule on this. Each chapter should go in its own separate ‘`.tex`’ file and they usually are split as:

- Chapter 1: Introduction to the thesis topic
- Chapter 2: Background information and theory
- Chapter 3: (Laboratory) experimental setup
- Chapter 4: Details of experiment 1

- Chapter 5: Details of experiment 2
- Chapter 6: Discussion of the experimental results
- Chapter 7: Conclusion and future directions

This chapter layout is specialised for the experimental sciences.

Figures – this folder contains all figures for the thesis. These are the final images that will go into the thesis document.

Primitives – this is the folder that contains scraps, particularly because one final image in the ‘Figures’ folder may be made from many separate images and photos, these source images go here. This keeps the intermediate files separate from the final thesis figures.

4.2.2 Files

Included are also several files, most of them are plain text and you can see their contents in a text editor. Luckily, many of them are auxiliary files created by L^AT_EX or BibTeX and which you don’t need to bother about:

Bibliography.bib – this is an important file that contains all the bibliographic information and references that you will be citing in the thesis for use with BibTeX. You can write it manually, but there are reference manager programs available that will create and manage it for you. Bibliographies in L^AT_EX are a large subject and you may need to read about BibTeX before starting with this.

Thesis.cls – this is an important file. It is the style file that tells L^AT_EX how to format the thesis. You will also need to open this file in a text editor and fill in your own information (such as name, department, institution). Luckily, this is not too difficult and is explained in section [4.3](#) on page [41](#).

Thesis.pdf – this is your beautifully typeset thesis (in the PDF file format) created by L^AT_EX.

Thesis.tex – this is an important file. This is the file that you tell L^AT_EX to compile to produce your thesis as a PDF file. It contains the framework and constructs that tell L^AT_EX how to layout the thesis. It is heavily commented so you can read exactly what each line of code does and why it is there. After you put your own information into the ‘Thesis.cls’ file, go to this file and begin filling it in – you have now started your thesis!

vector.sty – this is a L^AT_EX package, it tells L^AT_EX how to typeset mathematical vectors. Using this package is very easy and you can read the documentation on the site (you just need to look at the ‘vector.pdf’ file):

<http://www.ctan.org/tex-archive/macros/latex/contrib/vector/>

lstopatch.sty – this is a L^AT_EX package required by this LaTe_X template and is included as not all T_EX distributions have it installed by default. You do not need to modify this file.

Files that are *not* included, but are created by L^AT_EX as auxiliary files include:

Thesis.aux – this is an auxiliary file generated by L^AT_EX, if it is deleted L^AT_EX simply regenerates it when you run the main ‘.tex’ file.

Thesis.bbl – this is an auxiliary file generated by BibTeX, if it is deleted, BibTeX simply regenerates it when you run the main tex file. Whereas the ‘.bib’ file contains all the references you have, this ‘.bbl’ file contains the references you have actually cited in the thesis and is used to build the bibliography section of the thesis.

Thesis.blg – this is an auxiliary file generated by BibTeX, if it is deleted BibTeX simply regenerates it when you run the main ‘.tex’ file.

Thesis.lof – this is an auxiliary file generated by L^AT_EX, if it is deleted L^AT_EX simply regenerates it when you run the main ‘.tex’ file. It tells L^AT_EX how to build the ‘List of Figures’ section.

Thesis.log – this is an auxiliary file generated by L^AT_EX, if it is deleted L^AT_EX simply regenerates it when you run the main ‘.tex’ file. It contains messages from L^AT_EX, if you receive errors and warnings from L^AT_EX, they will be in this ‘.log’ file.

Thesis.lot – this is an auxiliary file generated by L^AT_EX, if it is deleted L^AT_EX simply regenerates it when you run the main ‘.tex’ file. It tells L^AT_EX how to build the ‘List of Tables’ section.

Thesis.out – this is an auxiliary file generated by L^AT_EX, if it is deleted L^AT_EX simply regenerates it when you run the main ‘.tex’ file.

So from this long list, only the files with the ‘.sty’, ‘.bib’, ‘.cls’ and ‘.tex’ extensions are the most important ones. The other auxiliary files can be ignored or deleted as L^AT_EX and BibTeX will regenerate them.

4.3 Filling in the ‘`Thesis.cls`’ File

You will need to personalise the thesis template and make it your own by filling in your own information. This is done by editing the ‘`Thesis.cls`’ file in a text editor.

Open the file and scroll down, past all the ‘\newcommand...’ items until you see the entries for ‘University Name’, ‘Department Name’, etc....

Fill out the information about your group and institution and ensure you keep to block capitals where it asks you to. You can also insert web links, if you do, make sure you use the full URL, including the ‘`http://`’ for this.

The last item you should need to fill in is the Faculty Name (in block capitals). When you have done this, save the file and recompile ‘`Thesis.tex`’. All the information you filled in should now be in the PDF, complete with web links. You can now begin your thesis proper!

4.4 The ‘`Thesis.tex`’ File Explained

The `Thesis.tex` file contains the structure of the thesis. There are plenty of written comments that explain what pages, sections and formatting the L^AT_EX code is creating. Initially there seems to be a lot of L^AT_EX code, but this is all formatting, and it has all been taken care of so you don’t have to do it.

Begin by checking that your information on the title page is correct. For the thesis declaration, your institution may insist on something different than the text given. If this is the case, just replace what you see with what is required.

Then comes a page which contains a funny quote. You can put your own, or quote your favourite scientist, author, person, etc... Make sure to put the name of the person who you took the quote from.

Next comes the acknowledgements. On this page, write about all the people who you wish to thank (not forgetting parents, partners and your advisor/supervisor).

The contents pages, list of figures and tables are all taken care of for you and do not need to be manually created or edited. The next set of pages are optional and can be deleted since they are for a more technical thesis: insert a list of abbreviations you have used in the thesis, then a list of the physical constants and numbers you refer to and finally, a list of mathematical symbols used in any formulae. Making the effort to fill these tables means the reader has a one-stop place to refer to instead of searching the

internet and references to try and find out what you meant by certain abbreviations or symbols.

The list of symbols is split into the Roman and Greek alphabets. Whereas the abbreviations and symbols ought to be listed in alphabetical order (and this is *not* done automatically for you) the list of physical constants should be grouped into similar themes.

The next page contains a one line dedication. Who will you dedicate your thesis to?

Finally, there is the section where the chapters are included. Uncomment the lines (delete the '%' character) as you write the chapters. Each chapter should be written in its own file and put into the ‘Chapters’ folder and named ‘`Chapter1`’, ‘`Chapter2`’, etc... Similarly for the appendices, uncomment the lines as you need them. Each appendix should go into its own file and placed in the ‘Appendices’ folder.

After the preamble, chapters and appendices finally comes the bibliography. The bibliography style (called ‘`unsrtnat`’) is used for the bibliography and is a fully featured style that will even include links to where the referenced paper can be found online. Do not under estimate how grateful your reader will be to find that a reference to a paper is just a click away. Of course, this relies on you putting the URL information into the BibTeX file in the first place.

4.5 Thesis Features and Conventions

To get the best out of this template, there are a few conventions that you may want to follow.

One of the most important (and most difficult) things to keep track of in such a long document as a thesis is consistency. Using certain conventions and ways of doing things (such as using a Todo list) makes the job easier. Of course, all of these are optional and you can adopt your own method.

4.5.1 Printing Format

This thesis template is designed for single sided printing as most theses are printed and bound this way. This means that the left margin is always wider than the right (for binding). Four out of five people will now judge the margins by eye and think, “I never noticed that before.”.

The headers for the pages contain the page number on the right side (so it is easy to flick through to the page you want) and the chapter name on the left side.

The text is set to 11 point and a line spacing of 1.3. Generally, it is much more readable to have a smaller text size and wider gap between the lines than it is to have a larger text size and smaller gap. Again, you can tune the text size and spacing should you want or need to. The text size can be set in the options for the ‘`\documentclass`’ command at the top of the ‘`Thesis.tex`’ file and the spacing can be changed by setting a different value in the ‘`\setstretch`’ commands (scattered throughout the ‘`Thesis.tex`’ file).

4.5.2 Using US Letter Paper

The paper size used in the template is A4, which is a common – if not standard – size in Europe. If you are using this thesis template elsewhere and particularly in the United States, then you may have to change the A4 paper size to the US Letter size. Unfortunately, this is not as simple as replacing instances of ‘`a4paper`’ with ‘`letterpaper`’.

This is because the final PDF file is created directly from the L^AT_EX source using a program called ‘pdfTeX’ and in certain conditions, paper size commands are ignored and all documents are created with the paper size set to the size stated in the configuration file for pdfTeX (called ‘`pdftex.cfg`’).

What needs to be done is to change the paper size in the configuration file for pdfTeX to reflect the letter size. There is an excellent tutorial on how to do this here:

http://www.physics.wm.edu/~norman/latexhints/pdf_papersize.html

It may be sufficient just to replace the dimensions of the A4 paper size with the US Letter size in the `pdftex.cfg` file. Due to the differences in the paper size, the resulting margins may be different to what you like or require (as it is common for Institutions to dictate certain margin sizes). If this is the case, then the margin sizes can be tweaked by opening up the `Thesis.cls` file and searching for the line beginning with, ‘`\setmarginsrb`’ (not very far down from the top), there you will see the margins specified. Simply change those values to what you need (or what looks good) and save. Now your document should be set up for US Letter paper size with suitable margins.

4.5.3 References

The ‘`natbib`’ package is used to format the bibliography and inserts references such as this one [41]. The options used in the ‘`Thesis.tex`’ file mean that the references are listed in numerical order as they appear in the text. Multiple references are rearranged

in numerical order (e.g. [42, 43]) and multiple, sequential references become reformatted to a reference range (e.g. [44]). This is done automatically for you. To see how you use references, have a look at the ‘`Chapter1.tex`’ source file. Many reference managers allow you to simply drag the reference into the document as you type.

Scientific references should come *before* the punctuation mark if there is one (such as a comma or period). The same goes for footnotes¹. You can change this but the most important thing is to keep the convention consistent throughout the thesis. Footnotes themselves should be full, descriptive sentences (beginning with a capital letter and ending with a full stop).

To see how `LATEX` typesets the bibliography, have a look at the very end of this document (or just click on the reference number links).

4.5.4 Figures

There will hopefully be many figures in your thesis (that should be placed in the ‘Figures’ folder). The way to insert figures into your thesis is to use a code template like this:

```
\begin{figure}[htbp]
    \centering
    \includegraphics{Figures/Electron.pdf}
    \rule{35em}{0.5pt}
    \caption[An Electron]{An electron (artist's impression).}
    \label{fig:Electron}
\end{figure}
```

Also look in the source file. Putting this code into the source file produces the picture of the electron that you can see in the figure below.

Sometimes figures don’t always appear where you write them in the source. The placement depends on how much space there is on the page for the figure. Sometimes there is not enough room to fit a figure directly where it should go (in relation to the text) and so `LATEX` puts it at the top of the next page. Positioning figures is the job of `LATEX` and so you should only worry about making them look good!

Figures usually should have labels just in case you need to refer to them (such as in Figure 4.1). The ‘`\caption`’ command contains two parts, the first part, inside the square brackets is the title that will appear in the ‘List of Figures’, and so should

¹Such as this footnote, here down at the bottom of the page.



FIGURE 4.1: An electron (artist's impression).

be short. The second part in the curly brackets should contain the longer and more descriptive caption text.

The ‘\rule’ command is optional and simply puts an aesthetic horizontal line below the image. If you do this for one image, do it for all of them.

The L^AT_EX Thesis Template is able to use figures that are either in the PDF or JPEG file format.

4.5.5 Typesetting mathematics

If your thesis is going to contain heavy mathematical content, be sure that L^AT_EX will make it look beautiful, even though it won’t be able to solve the equations for you.

The “Not So Short Introduction to L^AT_EX” (available [here](#)) should tell you everything you need to know for most cases of typesetting mathematics. If you need more information, a much more thorough mathematical guide is available from the AMS called, “A Short Math Guide to L^AT_EX” and can be downloaded from:

<ftp://ftp.ams.org/pub/tex/doc/amsmath/short-math-guide.pdf>

There are many different L^AT_EX symbols to remember, luckily you can find the most common symbols [here](#). You can use the web page as a quick reference or crib sheet and because the symbols are grouped and rendered as high quality images (each with a downloadable PDF), finding the symbol you need is quick and easy.

You can write an equation, which is automatically given an equation number by L^AT_EX like this:

```
\begin{equation}
E = mc^2
\label{eqn:Einstein}
\end{equation}
```

This will produce Einstein's famous energy-matter equivalence equation:

$$E = mc^2 \tag{4.1}$$

All equations you write (which are not in the middle of paragraph text) are automatically given equation numbers by L^AT_EX. If you don't want a particular equation numbered, just put the command, '\nonumber' immediately after the equation.

4.6 Sectioning and Subsectioning

You should break your thesis up into nice, bite-sized sections and subsections. L^AT_EX automatically builds a table of Contents by looking at all the '\chapter{}', '\section{}' and '\subsection{}' commands you write in the source.

The table of Contents should only list the sections to three (3) levels. A '\chapter{}' is level one (1). A '\section{}' is level two (2) and so a '\subsection{}' is level three (3). In your thesis it is likely that you will even use a '\subsubsection{}', which is level four (4). Adding all these will create an unnecessarily cluttered table of Contents and so you should use the '\subsubsection*{}' command instead (note the asterisk). The asterisk (*) tells L^AT_EX to omit listing the subsubsection in the Contents, keeping it clean and tidy.

4.7 In Closing

You have reached the end of this mini-guide. You can now rename or overwrite this pdf file and begin writing your own 'Chapter1.tex' and the rest of your thesis. The easy

work of setting up the structure and framework has been taken care of for you. It's now your job to fill it out!

Good luck and have lots of fun!

Guide written by —
Sunil Patel: www.sunilpatel.co.uk

Appendix A

Appendix Title Here

Write your Appendix content here.

Bibliography

- [1] Albert-László Barabási et al. Scale-free networks: a decade and beyond. *Science*, 325(5939):412–413, 2009.
- [2] Mikail Rubinov and O. Sporns. Complex network measures of brain connectivity: uses and interpretations. *NeuroImage*, 52(3):1059–1069, 2010.
- [3] Karl J Friston. Functional and effective connectivity in neuroimaging: a synthesis. *Human brain mapping*, 2(1-2):56–78, 1994.
- [4] Vito Latora and Massimo Marchiori. Efficient behavior of small-world networks. *Phys. Rev. Lett.*, 87(19):198701, 2001. doi: 10.1103/physrevlett.87.198701.
- [5] D. J. Watts and S. H. Strogatz. Collective dynamics of ‘small-world’ networks. *Nature*, 393:440–442, 1998.
- [6] M. E. J. Newman. The structure and function of complex networks. *SIAM Review*, 45(2):167–256, 2003. doi: 10.1137/s0036144503.
- [7] Mark D Humphries and Kevin Gurney. Network ‘small-world-ness’ : a quantitative method for determining canonical network equivalence. *PLoS One*, 3(4):e0002051, 2008.
- [8] E. T. Bullmore and O. Sporns. Complex brain networks: graph theoretical analysis of structural and functional systems. *Nat. Rev. Neurosci.*, 10(3):186–198, 2009.
- [9] Mikail Rubinov, O. Sporns, Cees Van Leeuwen, and M. Breakspear. Symbiotic relationship between brain structure and dynamics. *BMC Neuroscience*, 10(1):55, 2009.
- [10] M. P. van den Heuvel and O. Sporns. Rich-club organization of the human connectome. *The Journal of Neuroscience*, 31(44):15775–15786, 2011.
- [11] V. Vuksanović and P. Hövel. Functional connectivity of distant cortical regions: Role of remote synchronization and symmetry in interactions. *NeuroImage*, 97:1–8, 2014. doi: 10.1016/j.neuroimage.2014.04.039.

- [12] E. T. Bullmore and D. S. Bassett. Brain graphs: graphical models of the human brain connectome. *Annual review of clinical psychology*, 7:113–140, 2011.
- [13] N. Tzourio-Mazoyer, B. Landeau, D. Papathanassiou, F. Crivello, O. Etard, N. Delcroix, B. Mazoyer, and M. Joliot. Automated anatomical labeling of activations in SPM using a macroscopic anatomical parcellation of the MNI MRI single-subject brain. *Neuroimage*, 15(1):273–289, 2002.
- [14] Yasser Iturria-Medina, Roberto C Sotero, Erick J Canales-Rodríguez, Yasser Alemán-Gómez, and Lester Melie-García. Studying the human brain anatomical network via diffusion-weighted mri and graph theory. *Neuroimage*, 40(3):1064–1076, 2008.
- [15] Mingrui Xia, Jinhui Wang, and Yong He. Brainnet viewer: a network visualization tool for human brain connectomics. *PLoS One*, 8(7):e68910, 2013.
- [16] A. L. Barabasi and R. Albert. Emergence of scaling in random networks. *Science*, 286:509, 1999.
- [17] Randy L Buckner, Jorge Sepulcre, Tanveer Talukdar, Fenna M Krienen, Hesheng Liu, Trey Hedden, Jessica R Andrews-Hanna, Reisa A Sperling, and Keith A Johnson. Cortical hubs revealed by intrinsic functional connectivity: mapping, assessment of stability, and relation to alzheimer’s disease. *The Journal of Neuroscience*, 29(6):1860–1873, 2009.
- [18] J S Damoiseaux and Michael D Greicius. Greater than the sum of its parts: a review of studies combining structural connectivity and resting-state functional connectivity. *Brain Structure and Function*, 213(6):525–533, 2009.
- [19] M. E. J. Newman. *Networks: an introduction*. Oxford University Press, Inc., New York, 2010.
- [20] B Biswal, F Z Yetkin, V M Haughton, and J S Hyde. Functional connectivity in the motor cortex of resting human brain using echo-planar mri. *Magnetic Resonance in Medicine*, 34(4):537–541, 1995.
- [21] J S Damoiseaux, S A R B Rombouts, F Barkhof, P Scheltens, C. J. Stam, S M Smith, and C F Beckmann. Consistent resting-state networks across healthy subjects. *Proc. Natl. Acad. Sci. U.S.A.*, 103(37):13848–13853, 2006.
- [22] J. L. Vincent, G. H. Patel, M. D. Fox, A. Z. Snyder, J. T. Baker, D. C. Van Essen, J. M. Zempel, L. H. Snyder, M. Corbetta, and M. E. Raichle. Intrinsic functional architecture in the anaesthetized monkey brain. *Nature*, 447(7140):83–86, 2007.

- [23] V. Vuksanović and P. Hövel. Large-scale neural network model for functional networks of the human cortex. In A. Pelster and G Wunner, editors, *Selforganization in Complex Systems: The Past, Present, and Future of Synergetics, Proc. of the International Symposium, Hanse Institute of Advanced Studies Delmenhorst*, Berlin, 2014. Springer.
- [24] R. FitzHugh. Impulses and physiological states in theoretical models of nerve membrane. *Biophys. J.*, 1:445–466, 1961.
- [25] J. Nagumo, S. Arimoto, and S. Yoshizawa. An active pulse transmission line simulating nerve axon. *Proc. IRE*, 50:2061–2070, 1962.
- [26] A. Ghosh, Y. Rho, A. R. McIntosh, R. Kötter, and V. K. Jirsa. Noise during rest enables the exploration of the brain’s dynamic repertoire. *PLoS Comput Biol*, 4(10):e1000196, 2008. doi: 10.1371/journal.pcbi.1000196.
- [27] A. Ghosh, Y Rho, A R McIntosh, R Kötter, and V. K. Jirsa. Cortical network dynamics with time delays reveals functional connectivity in the resting brain. *Cogn. Neurodyn.*, 2(2):115–120, 2008. doi: 10.1007/s11571-008-9044-2.
- [28] G. Deco, V. K. Jirsa, A. R. McIntosh, O. Sporns, and R. Kötter. Key role of coupling, delay, and noise in resting brain fluctuations. *Proc. Natl. Acad. Sci. U.S.A.*, 106(25):10302–10307, 2009. doi: 10.1073/pnas.0901831106.
- [29] K. Friston, A Mechelli, R Turner, and C J Price. Nonlinear responses in fMRI: The balloon model, Volterra kernels, and other hemodynamics. *NeuroImage*, 12(4):466–477, 2000.
- [30] Marcus Kaiser and C. C. Hilgetag. Nonoptimal component placement, but short processing paths, due to long-distance projections in neural systems. *PLoS Comput. Biol.*, 2(7):e95, 2006.
- [31] V. Flunkert and E. Schöll. pydelay – a python tool for solving delay differential equations. arXiv:0911.1633 [nlin.CD], 2009.
- [32] P. Bogacki and L. F. Shampine. A 3(2) pair of runge - kutta formulas. *Applied Mathematics Letters*, 2(4):321–325, 1989. ISSN 0893-9659. doi: doi:10.1016/0893-9659(89)90079-7.
- [33] Richard B Buxton, Eric C Wong, and Lawrence R Frank. Dynamics of blood flow and oxygenation changes during brain activation: the balloon model. *Magnetic resonance in medicine*, 39(6):855–864, 1998.

- [34] Nicholas P Blockley, Valerie EM Griffeth, Aaron B Simon, and Richard B Buxton. A review of calibrated blood oxygenation level-dependent (bold) methods for the measurement of task-induced changes in brain oxygen metabolism. *NMR in Biomedicine*, 26(8):987–1003, 2013.
- [35] Anil K Seth, Paul Chorley, and Lionel C Barnett. Granger causality analysis of fmri bold signals is invariant to hemodynamic convolution but not downsampling. *Neuroimage*, 65:540–555, 2013.
- [36] Katsumi Irikura, Kenneth I Maynard, and Michael A Moskowitz. Importance of nitric oxide synthase inhibition to the attenuated vascular responses induced by topical l-nitroarginine during vibrissal stimulation. *Journal of Cerebral Blood Flow & Metabolism*, 14(1):45–48, 1994.
- [37] John Mayhew, Dewen Hu, Ying Zheng, Steven Askew, Yuqian Hou, Jason Berwick, Peter J Coffey, and Nicky Brown. An evaluation of linear model analysis techniques for processing images of microcirculation activity. *Neuroimage*, 7(1):49–71, 1998.
- [38] KL Miller, WM Luh, TT Liu, A Martinez, T Obata, EC Wong, LR Frank, and RB Buxton. Characterizing the dynamic perfusion response to stimuli of short duration. 8:580, 2000.
- [39] Karl J Friston, Oliver Josephs, Geraint Rees, and Robert Turner. Nonlinear event-related responses in fmri. *Magnetic resonance in medicine*, 39(1):41–52, 1998.
- [40] Joseph B Mandeville, John JA Marota, C Ayata, Greg Zaharchuk, Michael A Moskowitz, Bruce R Rosen, and Robert M Weisskoff. Evidence of a cerebrovascular postarteriole windkessel with delayed compliance. *Journal of Cerebral Blood Flow & Metabolism*, 19(6):679–689, 1999.
- [41] V. N. Abakumov, L. N. Kreshchuk, and I. N. Yassievich. Carrier capture by attractive centers in strong electric fields. *Sov. Phys. Semicond.*, 12(2):152, 1977.
- [42] V. N. Abakumov, V. I. Perel, and I. N. Yassievich. Capture of carriers by attractive centers in semiconductors. *Sov. Phys. Semicond.*, 12(1):1, 1978.
- [43] H. D. I. Abarbanel, N. F. Rulkov, and M. M. Sushchik. Generalized synchronization of chaos: The auxiliary system approach. *Phys. Rev. E*, 53(5):4528–4535, 1996.
- [44] V. N. Biktashev and A. V. Holden. Design principles of a low voltage cardiac defibrillator based on the effect of feedback resonant drift. *J. Theor. Biol.*, 169(2):101–112, 1994.